Partitioning of Diluted Anyons Reveals their Braiding Statistics

June-Young M. Lee[1*], Changki Hong[2*], Tomer Alkalay[2*], Noam Schiller[2], Vladimir Umansky[2],

Moty Heiblum[2], Yuval Oreg[2], H.-S. Sim[1]

[1]Department of Physics, Korea Advanced Institute of Science and Technology, Daejeon 34141, South Korea

[2]Department of Condensed Matter, Weizmann Institute of Science, Rehovot, Israel

*Equal Contribution

Correspondent Authors:
H.-S. Sim……hs_sim@kaist.ac.kr
Moty Heiblum….moty.heiblum@weizmann.ac.il

ABSTRACT

Correlations of partitioned particles carry essential information about their quantumness [1]. Partitioning *full* beams of charged particles leads to current fluctuations, with their autocorrelation (AC, shot noise) revealing the particles' charge [2]. This is not the case when the partitioned particle beams are *diluted*. Bosons or fermions will exhibit particles antibunching (due to their discreteness) [3, 4]. However, when partitioning anyons, such as the quasiparticles in fractional quantum Hall states (FQH), the AC unveils an essential aspect of their exchange statistics: their 'braiding phase' [5]. Here, we describe detailed measurements of partitioning diluted anyonic edge modes of the FQH 1/3-state. The measured excess AC agrees with our theory of braiding in the 'time-domain' - with a braiding angle of 2θ=$2\pi/3$ - without any fitting parameters. Our work offers a relatively straightforward and simple method to observe the braiding statistics of other exotic states, such as non-abelian states, without resorting to complex interference experiments [6].

Fractional quantum Hall systems host exotic quasiparticles (QPs) called anyons that carry fractional charges and obey fractional statistics. An adiabatic braiding of abelian anyons leads to an added fractional statistical phase 2θ, while for non-abelian anyons, the original state transforms to another degenerate state [7-9]. The QP's charge is determined from the partitioned *full* beam's excess shot noise (autocorrelation of charge fluctuations, AC) [2]. Here, we demonstrate that the Fano factor of the AC of a partitioned *dilute beam* of anyons reveals their braiding phase.

The traditional strategy to observe the statistics of QPs of FQH states involves interference in a Fabry-Perot Interferometer [10] or a Mach-Zehnder Interferometer [11], where edge modes circulate localized QPs in the insulating bulk. Another recent approach [12] exploited a configuration of three quantum point contacts (QPCs) where two highly dilute beams, partitioned by two side-QPCs, 'collided' at a central QPC (a typical HOM configuration [13, 14]). Measured for the anyonic 1/3 FQH state, the cross-correlation (CC) of the back-scattered QPs beams was interpreted as a partly anyonic-bunching at the central QPC [12, 15].

A different origin of the 'three-QPC' outcome is based on braiding in the 'time domain' between the two impinging dilute anyons and the thermally (or vacuum) excited 'particle-hole' anyons at the central QPC [5, 6]. To test this scenario, we focused on a 'two-QPC geometry' where one QPC dilutes the anyon beam, which another QPC further partitions, thus resulting in shot noise (AC). Testing under different conditions, such as beam dilution, second QPC's transmission, and beam travel distance, we found an anomalous AC with a Fano factor ($\mathcal{F}_{\text{dilute}}$) that agrees with our theory of time-domain braiding at the partitioning QPC (without fitting parameters).

Notably, while the theoretical description of the time-domain anyon braiding in a QPC is based on the chiral Luttinger liquid (CLL) theory, or the equivalent conformal field theory [5, 6], the 'saddle potential' in a partly pinched QPC [16] is far from the ideal barrier in the CLL theory. To overcome this difficulty, we developed a theoretical description that hybridizes the CLL theory and a phenomenological theory in the spirit of the successful ubiquitous approach of fractional charge determination via AC measurement [2].

Our experimental setup is shown in Fig. 1(a) (Supplementary Sec. I). The source (S) is biased by voltage V_{S}, injecting a *full* QPs beam with current $I_{\text{S}} = GV_S$, flowing chirally along Edge1, with conductance $G = \nu e^2/h$ at filling factor $\nu = 1/3$. The full beam is highly diluted by QPC1, with a reflection probability R_{QPC1} and average current $I_{\text{QPC1}} = I_{\text{S}} R_{\text{QPC1}}$. The dilute beam flows chirally along Edge2, impinging at QPC2 (being $2\mu m$ away), where it is further partitioned. The scattered current fluctuations are measured after being amplified by amplifiers A and B; obtaining the excess AC spectral densities S_{A} & S_{B} and the CC S_{AB}. The diluted quasiparticles charge e^* was determined from the shot noise measurement in QPC1 by comparing the experimental results and the phenomenological expression of the spectral density [2, 17, 18],

$$S_{\text{QPC1}} = 2e^* I_{\text{S}} R_{\text{QPC1}} (1 - R_{\text{QPC1}}) \left[\coth\left(\frac{e^* V_{\text{S}}}{2k_B T}\right) - \frac{2k_B T}{e^* V_{\text{S}}} \right] . \tag{1}$$

Here, S_{QPC1} is the excess AC in QPC1, which can also be obtained by $S_{\text{QPC1}} = S_{\text{A}} + S_{\text{B}} + 2S_{\text{AB}}$ (Fig. 1(b)). The data agrees nicely with $e^* = e/3$ (a similar measurement was performed in QPC2, Supplementary Sec. II).

We now elaborate on the phenomenological hybridization of the non-interacting expression in Eq. (1) and the interacting theory of the CLL. In the limit of very large V_{S}/T and very small R_{QPC1}, Eq. (1) agrees with the prediction of the CLL theory. In the latter, the current and shot noise are expressed as $I_{\text{QPC1}} = e^*(W_{1\to2} - W_{2\to1})$ and $S_{\text{QPC1}} = 2e^{*2}(W_{1\to2} + W_{2\to1})$, where $W_{i\to j}$ is the tunneling rate of an anyon from Edge***i*** to Edge***j***. When the full biased beam obeys $e^* V_S \gg k_B T$, the rate $W_{2\to1}$ is exponentially suppressed in comparison with $W_{1\to2}$, resulting in $S_{\text{QPC1}} = 2e^* I_{\text{QPC1}}$. The phenomenological binomial factor $(1 - R_{\text{QPC1}})$ in Eq. (1) relates to charge fluctuation at a QPC with non-interacting particles. The temperature-dependent term emanates from the detailed balance principle [18].

We extend Eq. (1) to the two-QPC geometry. When a *dilute* beam is partitioned by QPC2, the spectral density S_{QPC2} of the excess AC of current fluctuations in QPC2 can be expressed as,

$$S_{\text{QPC2}} = \mathcal{F}_{\text{dilute}} \times 2e^* I_{\text{QPC1}} R_{\text{QPC2}} (1 - R_{\text{QPC2}}) \left[\coth\left(\frac{e^* V_{\text{S}}}{2k_B T}\right) - \frac{2k_B T}{e^* V_{\text{S}}} \right] , \tag{2}$$

with $\mathcal{F}_{\text{dilute}}$ being dependent on the diluting R_{QPC1} of the beam (Supplementary Sec. III). R_{QPC2} is the reflection probability of QPC2. This expression has the same structure as Eq. (1), with the replacement of $I_{\text{S}} \leftrightarrow I_{\text{QPC1}}$ and $R_{\text{QPC1}} \leftrightarrow R_{\text{QPC2}}$.

The Fano factor $\mathcal{F}_{\text{dilute}}$ distinguishes between different partitioning processes. We consider the limits of large V_{S}, small R_{QPC2}, dilute current $I_{\text{QPC2}} = I_{\text{QPC1}} R_{\text{QPC2}}$ and spectral density $S_{\text{QPC2}} = \mathcal{F}_{\text{dilute}} \times 2e^* I_{\text{QPC2}}$. In these limits, $I_{\text{QPC2}} = e^*(W_{2\to3} - W_{3\to2})$, with spectral density $S_{\text{QPC2}} = 2e^{*2}(W_{2\to3} + W_{3\to2})$, and $\mathcal{F}_{\text{dilute}} = (W_{2\to3} + W_{3\to2})/(W_{2\to3} - W_{3\to2})$. Among possible partitioning processes, we first consider the trivial partitioning where an anyon in the dilute beam directly tunnels at QPC2 from Edge2 to Edge3 (Fig. 2(a)). This ubiquitous partitioning manifests particle antibunching [3, 4], regardless of whether the particle is a boson, a fermion, or an anyon. Here $\mathcal{F}_{\text{dilute}} = 1$ since the rate $W_{2\to3}$ exponentially dominates $W_{3\to2}$ at high enough voltage ($e^* V_S \gg k_B T$), in a similar fashion to the partitioning of a full beam.

However, the CLL theory does not support the trivial partitioning process of highly diluted anyonic beams. Yet, it predicts another process involving anyon braiding [5, 6]. In this process, which we call 'time-domain' braiding, the anyon that tunnels at QPC2 is not the arriving anyon of the dilute beam but a thermally excited (or vacuum excited) anyon. The excited anyon tunnels between Edge2 and Edge3 at time t_1, leaving a hole behind. This anyon tunnels back at time t_2 and is 'pair-annihilated' with the hole. This time-domain loop of the excited anyon in QPC2 braids with arriving anyons in the diluted beam during the time interval $t_2 - t_1$ (Fig. 2(b)). This braiding process leads to the modified Fano factor $\mathcal{F}_{\text{dilute}}$ (Methods and Supplementary Sec. III),

$$\mathcal{F}_{\text{dilute}} = -\cot \pi\delta \cot\left(\left(\frac{\pi}{2} - \theta\right)(2\delta - 1)\right) \simeq 3.27, \tag{3}$$

when $R_{\text{QPC1}} \ll 1$. Here, δ is the 'scaling dimension' of anyon tunneling at QPC2 and 2θ ($\neq 0, 2\pi$) is the braiding angle. The value $\mathcal{F}_{\text{dilute}}$=3.27 is obtained with the ideal ν=1/3 state, with the corresponding δ=1/3 and θ=π/3.

Since measuring the excess AC of a highly diluted beam is challenging, we developed a phenomenological theory for 'moderately diluted' beams. Going beyond the CLL theory, the critical step is the identification of the average braiding phase in the time-domain braiding process,

$$\langle e^{2ik\theta} \rangle_{\text{binomial}} = \sum_{k=0}^{n} P_k \, e^{2ik\theta} = \left(1 - R_{\text{QPC1}} + R_{\text{QPC1}} e^{2i\theta}\right)^n, \tag{4}$$

here, k denotes the number of anyons in the dilute beam which arrive at QPC2 in the time interval $t_2 - t_1$. The phase term $e^{2ik\theta}$ corresponds to the braiding phase of a thermally excited anyon with each of these anyons. The probability P_k of the k's anyon event is naturally assumed to follow the binomial distribution $P_k = \frac{n!}{k!\,(n-k)!}(R_{\text{QPC1}})^k(1 - R_{\text{QPC1}})^{n-k}$, i.e., the probability for k anyons being reflected by QPC1, with reflection probability R_{QPC1}. The maximum value of k is determined by $n = I_{\text{S}}(t_2 - t_1)/e^*$. The average braiding phase is implemented in the calculation of $\mathcal{F}_{\text{dilute}}$ employing the ideal CLL parameters δ=1/3, the braiding angle 2θ=2π/3 at ν=1/3, and integrating over $t_2 - t_1$. As the beam is less diluted (i.e., fuller), the trivial partitioning process is also considered in the above expression, though its contribution is small (Methods and Supplementary Sec. III). Note that the average braiding phase is trivial, $\langle e^{2ik\theta} \rangle_{\text{binomial}} = 1$ for fermions ($\theta = \pi$) or bosons ($\theta = 0$).

We measured the excess spectral density S_{B} of the excess AC for two injection cases: a *full* beam and a *dilute* beam. We first performed these measurements in the integer regime (outer edge mode of filling 3). The Fano factors in both cases agree with trivial partitioning $\mathcal{F}_{\text{dilute}}=1$, with the expected electronic charge $e^*=e$ (Supplementary Sec. II). Similar measurements were performed with the anyonic quasiparticles (at filling 1/3), with the two cases exhibiting drastic differences. In the *full* beam case S_B follows the voltage dependence expression of Eq. (1), with a determined charge $e^*\simeq e/3$ (Supplementary Sec. II). In the dilute case, with $R_{\text{QPC1}}\approx 0.1$, the experimental value of the Fano factor, $\mathcal{F}_{\text{dilute}}$, was compared with that in Eq. (2), utilizing the fact that S_B coincides with S_{QPC2} at large voltages (Supplementary Sec. IV). Noting that for $R_{\text{QPC1}}, R_{\text{QPC2}} \simeq 0.1 \ll 1$, the results are close to $\mathcal{F}_{\text{dilute}}\sim 3.27$, ruling out the trivial process ($\mathcal{F}_{\text{dilute}}=1$) and substantiating the time-domain braiding process (Eq. (4) and Fig. 3).

In Fig. 4, the spectral density S_B of the AC was measured with varying dilutions and different R_{QPC2}. With less dilution (fuller beam), the time-domain braiding process gives rise to smaller $\mathcal{F}_{\text{dilute}}$ and the trivial partitioning contributes more to $\mathcal{F}_{\text{dilute}}$, albeit still small. Notice the excellent agreement between the experimental data and the phenomenological theory over a wide range of V_S/T, R_{QPC1}, and R_{QPC2} without fitting parameters.

The time-domain braiding process requires phase coherence of the dilute beam of anyons [5, 6]. To test the assumption that the inter-QPC distance of $2\mu m$ is sufficiently shorter than the coherence length, we fabricated a similar geometry with an inter-QPC distance of $20\mu m$. In this case, the measured S_B showed clear deviation from $\mathcal{F}_{\text{dilute}}\sim 3.27$, following the trivial formalism of the extended Eq. (1) for non-interacting particles with $R_{\text{QPC1}} \rightarrow R_{\text{QPC1}}R_{\text{QPC2}}$ [19] (Fig. 5).

We extended our work to the filling $\nu = 2/5$ in the FQH regime (Supplementary Sec. V). Partitioning dilute anyons with $e^* = e/3$ (the outer edge mode) at QPC2, we find (theoretically) a Fano factor close to $\mathcal{F}_{\text{dilute}}\sim 3.27$, which supports the time-domain braiding with $2\theta = 2\pi/3$ and δ=1/3 as in $\nu = 1/3$. On the other hand, partitioning dilute anyons with charge $e^* = e/5$ (the inner edge mode) at QPC2, we find (theoretically) $\mathcal{F}_{\text{dilute}}\sim 1$, which is in our measurement's uncertainty (suffering from the very weak shot noise) with $R_{\text{QPC1}} = 0.088$, $R_{\text{QPC2}} = 0.186$, inter-QPC distance of $2\mu m$, and temperature T=39mK. The result is close to the Fano factor corresponding to the trivial partition process (see above).

It might be worthwhile to compare our two-QPC experiment with a recent work based on a three-QPC setup [12]. In the latter work, the measured CC (of the partitioned diluted 1/3 beam) was attributed to 'anyon-bunching by collision' following a classical lattice model [15], which differs from our interpretation. Consequently, we tested our theory by performing a three-QPC experiment and found the results agree well with our phenomenological approach (at a relatively large R_{QPC1}), supporting the underlying physics of the anyon braiding (Supplementary Sec. VI).

Here we propose and demonstrate a relatively simple experimental configuration that identifies the statistical phase of abelian anyons in the FQH regime. We present an experiment and a supporting theory in the 1/3 filling of the FQH. Our findings are also significant considering the long-time disagreements between experiments and the chiral Luttinger theory [20]. For example, the theoretical power-law voltage dependence of the reflection probability in a QPC, $R_{\text{QPC}} \propto V^{2\delta-2}$, has not been confirmed experimentally (Supplementary Sec. II). As such, it is worth examining the robustness of our Fano factor, $\mathcal{F}_{\text{dilute}}$, with respect to a variation in the scaling dimension, δ. We find that $\mathcal{F}_{\text{dilute}}$ is expected to vary only by 10% throughout the range $1/3 < \delta < 2/3$ (Supplementary Sec. III).

Our work demonstrates that due to the exotic anyonic statistics, thermally excited anyons (or vacuum fluctuations) in a single barrier are correlated with impinging diluted anyons. In other words, time-domain trajectories of the thermally excited anyons become topologically linked, i.e., braided, with those of the dilute anyons. This feat is accomplished by a relatively simple ‘two-QPC’ configuration – allowing a straightforward identification of the braiding phase in a considerably simpler method than interference experiments. Moreover, our work suggests a promising route toward observing the ‘topological order’ of non-abelian anyons, such as in the 5/2 filling in the FQH regime [6].

METHODS

Theory of the Fano factor $\mathcal{F}_{\text{dilute}}$

In the CLL theory and the equivalent conformal field theory [6], the time-domain braiding process is described by a non-equilibrium correlator $C_{\text{neq}}(t_1, t_2)$ of the anyon tunneling operator at QPC2 in the presence of a dilute anyon beam flowing to QPC2. It is expressed as $C_{\text{neq}}(t_1, t_2) = \langle e^{2ik\theta} \rangle_{\text{Poissonian}} C_{\text{eq}}(t_1, t_2)$ in the limit of a highly dilute beam, $R_{\text{QPC1}} \ll 1$, where $C_{\text{eq}}(t_1, t_2)$ is the equilibrium correlator in the absence of the dilute beam. Here, $\langle e^{2ik\theta} \rangle_{\text{Poissonian}} = \sum_{k=0}^{\infty} Q_k\, e^{2ik\theta}$ is the average of the braiding phase $e^{2ik\theta}$, which accumulates when the time-domain loop of thermally excited anyon braids with k anyons of the dilute beam arriving at QPC2 in the time interval $t_2 - t_1$. The probability Q_k represents k random anyon injections from Edge1 to Edge2 at QPC1 (see Figs. 1 & 2) over the time interval $t_2 - t_1$. For a highly diluted beam, it follows the Poisson distribution $Q_k = (m^k/k!)e^{-m}$, where $m = I_{\text{QPC1}}(t_2 - t_1)/e^*$.

It is naturally expected that in a less dilute (fuller) beam (with a relatively large R_{QPC1}, yet small enough for anyon tunneling), the distribution of anyons in the beam follows a binomial distribution rather than the Poissonian distribution. Hence, to describe the cases of less dilute beams, we replace the multiplicative factor $\langle e^{2ik\theta} \rangle_{\text{Poissonian}}$ by the average braiding phase $\langle e^{2ik\theta} \rangle_{\text{binomial}}$, with the latter averaged over the binomial distribution in Eq. (4). Then the correlator is,

$$C_{\text{neq}}(t_1, t_2) = \left(1 - R_{\text{QPC1}} + R_{\text{QPC1}} e^{2i\theta \operatorname{sign}(t_2 - t_1)}\right)^{\frac{I_S}{e^*}|t_1 - t_2|} C_{\text{eq}}(t_1, t_2). \tag{5}$$

In the dilute limit of $R_{\text{QPC1}} \ll 1$, the multiplicative factor $(1 - R_{\text{QPC1}} + R_{\text{QPC1}} e^{\pm 2i\theta})^{\frac{I_S}{e^*}|t_1 - t_2|}$ is reduced to the factor $e^{-(1 - e^{\pm 2i\theta})\frac{I_{\text{QPC1}}}{e^*}|t_1 - t_2|}$ found in previous work [6]. Employing $C_{\text{neq}}(t_1, t_2)$ with an integral over $t_2 - t_1$, it is straightforward to compute the rates of anyon tunneling (back and forth) at QPC2 in the time-domain braiding process. At zero temperature and $R_{\text{QPC2}} \ll 1$, we get,

$$\begin{aligned} W_{2\to3}^{\text{braid}} &\propto \operatorname{Re}\left[e^{i\pi\delta}\left(-\log\left(1 + R_{\text{QPC1}}\left(e^{-i2\theta} - 1\right)\right)\right)^{2\delta - 1}\right], \\ W_{3\to2}^{\text{braid}} &\propto \operatorname{Re}\left[e^{i\pi\delta}\left(-\log\left(1 + R_{\text{QPC1}}\left(e^{i2\theta} - 1\right)\right)\right)^{2\delta - 1}\right] \quad , \end{aligned} \tag{6}$$

with the full expressions given in Supplementary Sec. III. In contrast to the trivial process where $W_{3\to2}$ is exponentially suppressed in comparison with $W_{2\to3}$, both $W_{2\to3}^{\text{braid}}$ and $W_{3\to2}^{\text{braid}}$ are non-negligible in the time-domain braiding. The appearance of the combination $e^{\pm i2\theta} - 1$ in Eq. (6) implies that the rates $W_{2\to3}^{\text{braid}}$ and $W_{3\to2}^{\text{braid}}$ vanish, not contributing to the tunneling currents and noise at QPC2, in the cases of fermions ($\theta = \pi$) or bosons ($\theta = 0$). Hence the time-domain braiding does not exist with fermions or bosons, but only with anyons [21-24].

When the time-domain braiding process dominates over other processes, the Fano factor is written as,

$$\mathcal{F}_{\text{dilute}} = \frac{W_{2\to3}^{\text{braid}} + W_{3\to2}^{\text{braid}}}{W_{2\to3}^{\text{braid}} - W_{3\to2}^{\text{braid}}} = -\cot \pi\delta \frac{\operatorname{Re}\left[\left(-\log\left(1 + R_{\text{QPC1}}\left(e^{-i2\theta} - 1\right)\right)\right)^{2\delta - 1}\right]}{\operatorname{Im}\left[\left(-\log\left(1 + R_{\text{QPC1}}\left(e^{-i2\theta} - 1\right)\right)\right)^{2\delta - 1}\right]} \quad . \tag{7}$$

In the dilute limit of $R_{\mathrm{QPC1}} \ll 1$, we find $\mathcal{F}_{\mathrm{dilute}} \rightarrow -\cot\pi\delta \frac{\mathrm{Re}[(1-e^{-i2\theta})^{2\delta-1}]}{\mathrm{Im}[(1-e^{-i2\theta})^{2\delta-1}]}$ in Eq. (3). As the beam becomes less dilute, the trivial partitioning process contributes more to the rates of $W_{2\rightarrow3}^{\mathrm{triv}}$ and $W_{3\rightarrow2}^{\mathrm{triv}}$ (Supplementary Sec. III). Then the Fano factor $\mathcal{F}_{\mathrm{dilute}}$ is obtained according to all the rates accounted for all the processes, $W_{2\rightarrow3} = W_{2\rightarrow3}^{\mathrm{braid}} + W_{2\rightarrow3}^{\mathrm{triv}}$ and $W_{3\rightarrow2} = W_{3\rightarrow2}^{\mathrm{braid}} + W_{3\rightarrow2}^{\mathrm{triv}}$, with the experimentally measured R_{QPC1} as input of the calculation. We note that $W_{2\rightarrow3}^{\mathrm{triv}}$ and $W_{3\rightarrow2}^{\mathrm{triv}}$ are not negligible but much smaller than $W_{2\rightarrow3}^{\mathrm{braid}}$ and $W_{3\rightarrow2}^{\mathrm{braid}}$ for the values of R_{QPC1} studied in our experiments.

Author's contribution

JYML and HSS developed the theory and analyzed the data. CH and TA fabricated the structures, did all measurements and analyzed the data. NS and YO, added perspective on the theory. VU designed and grew the heterostructures by MBE. MH supervised the experiments.

Acknowledgments

J.Y.M.L. acknowledges support from Korea NRF, NRF-2019-Global Ph.D. fellowship. H.-S.S acknowledges support from Korea NRF, the SRC Center for Quantum Coherence in Condensed Matter (Grant No. 2016R1A5A1008184). N.S. acknowledges fruitful discussions with Yotam Shapira and Ady Stern, and. acknowledges the Clore Scholars Programme. Y.O. acknowledges the partially supported by grants from the ERC under the European Union's Horizon 2020 research and innovation programme (grant agreements LEGOTOP No. 788715 and HQMAT No. 817799), the DFG (CRC/Transregio 183, EI 519/7-1), the BSF and NSF (2018643), the ISF Quantum Science and Technology (2074/19). M.H. acknowledges the continuous support of the Sub-Micron Center staff, the support of the European Research Council under the European Community's Seventh Framework Program (FP7/2007-2013)/ERC under grant agreement number 713351.

References

[1] R. Hanbury Brown and R. Q. Twiss, A Test of a New Type of Stellar Interferometer on Sirius, Nature 178, 1046 (1956).

[2] R. de-Picciotto et al., Direct observation of a fractional charge, Nature 389, 162 (1997); L. Saminadayar et al., Observation of the e/3 fractionally charged Laughlin Quasiparticle, Phys. Rev. Lett. 79, 2526 (1997).

[3] H. J. Kimble, M. Dagenais, and L. Mandel, Photon Antibunching in Resonance Fluorescence, Phys. Rev. Lett. 39, 691 (1977).

[4] M. Henny et al., The Fermionic Hanbury Brown and Twiss Experiment, Science 284, 296 (1999); W. D. Oliver et al., Hanbury Brown and Twiss-Type Experiment with Electrons, Science 284, 299 (1999).

[5] B. Lee, C. Han, H.-S. Sim, Negative Excess Shot Noise by Anyon Braiding. Phys. Rev. Lett. 123, 016803 (2019).

[6] J.-Y. M. Lee and H.-S. Sim, Non-Abelian Anyon Collider, arXiv:2202.03649 (2022).

[7] J. M. Leinaas and J. Myrheim, On the theory of identical particles. Il Nuovo Cimento B Series **37**, 1 (1977).

[8] D. Arovas, J. R. Schrieffer, and F. Wilczek, Fractional statistics and the quantum Hall effect. Phys. Rev. Lett **53**, 722-723 (1984).

[9] C. Nayak, A. Stern, M. Freedman, and S. Das Sarma, Non-Abelian anyons and topological quantum computation. Rev. Mod. Phys. **80**, 1083 (2008).

[10] J. Nakamura et al., Direct observation of anyonic braiding statistics, Nat. Phys. 16, 931 (2020); C. de C. Chamon et al., Phys. Rev. B 55, 2331 (1997).

[11] H. K. Kundu et al., Anyonic interference and braiding phase in a Mach-Zehnder Interferometer, arXiv:2203.04205 (2022).

[12] H. Bartolomei et al., Fractional statistics in anyon collisions, Science 368, 6487 (2020).

[13] C. K. Hong, Z. Y. Ou, and L. Mandel, Measurement of subpicosecond time intervals between two photons by interference. Phys. Rev. Lett. 59, 2044 (1987).

[14] R. Liu et al., Quantum interference in electron collision, Nature 391, 263 (1998); E. Bocquillon et al., Coherence and indistinguishability of single electrons emitted by independent sources, Science 339, 1054 (2013).

[15] B. Rosenow, I. P. Levkivskyi, and B. I. Halperin, Current Correlations from a Mesoscopic Anyon Collider, Phys. Rev. Lett. 116, 156802 (2016).

[16] Y. C. Chung et al., Anomalous chiral Luttinger liquid behavior of diluted fractionally charged quasiparticles, Phys. Rev. B 67, 201104(R) (2003).

[17] For a review, see M. Heiblum, in Perspectives of Mesoscopic Physics: Dedicated to Yoseph Imry's 70th Birthday, edited by A. Ahrony and O. Entin-Wohlman (World Scientific, Singapore, 2010).

[18] D. E. Feldman and M. Heiblum, Why a noninteracting model works for shot noise in fractional charge experiments, Phys. Rev. B 95, 115308 (2017).

[19] Y. M. Blanter and M. Büttiker, Shot noise in mesoscopic conductors, Physics Reports 336, 1-116 (2000).

[20] D. C. Glattli, Tunneling Experiments in the Fractional Quantum Hall Regimes. In: Douçot, B., Pasquier, V., Duplantier, B., Rivasseau, V. (eds) The Quantum Hall Effect. Progress in Mathematical Physics, vol 45. Birkhäuser Basel (2005).

[21] C. Han, J. Park, Y. Gefen, and H.-S. Sim, Topological vacuum bubbles by anyon braiding. Nat. Commun. **7**, 11131 (2016).

[22] J.-Y. M. Lee, C. Han, and H.-S. Sim, Fractional Mutual Statistics on Integer Quantum Hall Edges. Phys. Rev. Lett. **125**, 196802 (2020).

[23] T. Morel, J.-Y. M. Lee, H.-S. Sim, and C. Mora, Fractionalization and anyonic statistics in the integer quantum Hall collider, Phys. Rev. B **105**, 075433 (2022).

[24] T. Jonckheere, J. Rech, B. Gr´emaud, and T. Martin, Anyonic statistics revealed by the hong-ou-mandel dip for fractional excitations, arXiv:2207.07172 (2022).

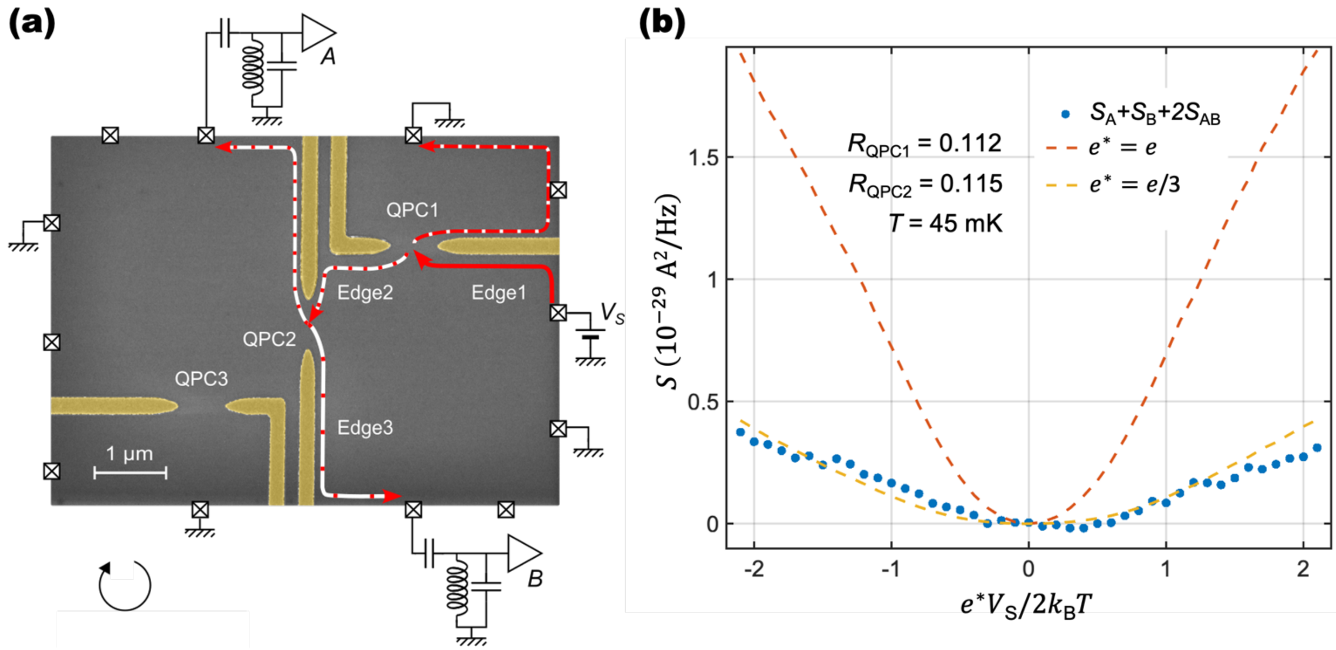

Figure 1. Partitioning diluted anyons in a two-QPC geometry. (a) The experimental setup. SEM image and edge modes. The QPC's metallic gates are colored in yellow. The ohmic contacts are more than a hundred micrometers away from the core structure. Source current propagates along Edge1 and is diluted by QPC1 with R_{QPC1}. The diluted beam reaches QPC2 fabricated 2μm away along Edge2. Partitioning takes place in QPC2 with back reflection along Edge3. Amplifiers measure the excess auto-correlation (AC) and the cross-correlation (CC). **(b)** Spectral density sum of auto-correlations and cross-correlation of the current fluctuation (shot noise) in QPC2 diluted by QPC1 (blue dots) – with charge $\boldsymbol{e^* = e/3}$ (blue dots – data; yellow dashed line - expected). $\boldsymbol{R_{QPC1} = 0.112}$, $\boldsymbol{R_{QPC2} = 0.115}$ and Temperature 45 mK (detail in Supplementary Sec. II). Charge $\boldsymbol{e^* = e}$ shown for comparison (red dashed line).

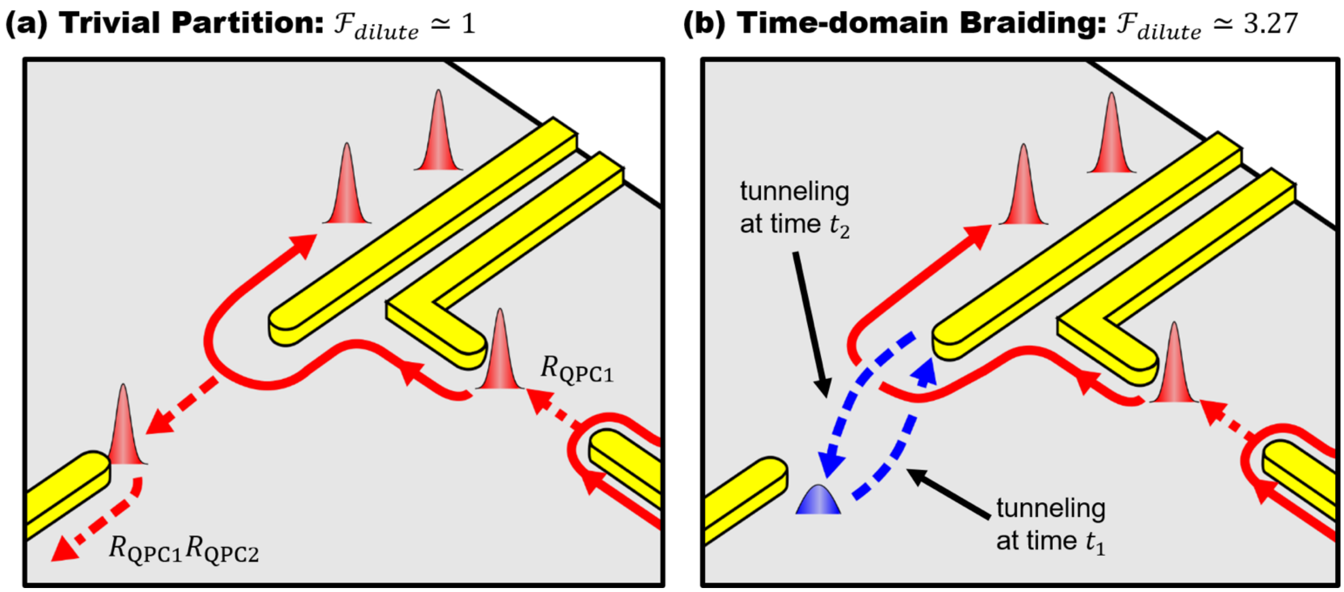

Figure 2. Trivial and braiding partitioning processes in QPC2. (a) Trivial partitioning: QPC1 dilutes the incoming beam by reflection R_{QPC1} (red wave packets), which is partitioned further in QPC2 by $\boldsymbol{R_{\mathrm{QPC2}}}$. Shot noise is proportional to $\boldsymbol{R_{\mathrm{QPC1}}R_{\mathrm{QPC2}}}$. **(b)** Time-domain braiding: QPC1 dilutes the incoming beam by reflection $\boldsymbol{R_{\mathrm{QPC1}}}$ (red wave-packets). Thermally activated particle-like anyon (leaving a hole) tunnels within QPC2 (blue arrow from one edge mode to another) at time $\boldsymbol{t_1}$. Diluted anyon arrived (with probability $\boldsymbol{R_{\mathrm{QPC1}}}$). The particle-anyon tunnels back at a later time $\boldsymbol{t_2}$ (blue dashed arrows), thus braiding the arriving diluted anyon during the interval time $\boldsymbol{t_2}$-$\boldsymbol{t_1}$.

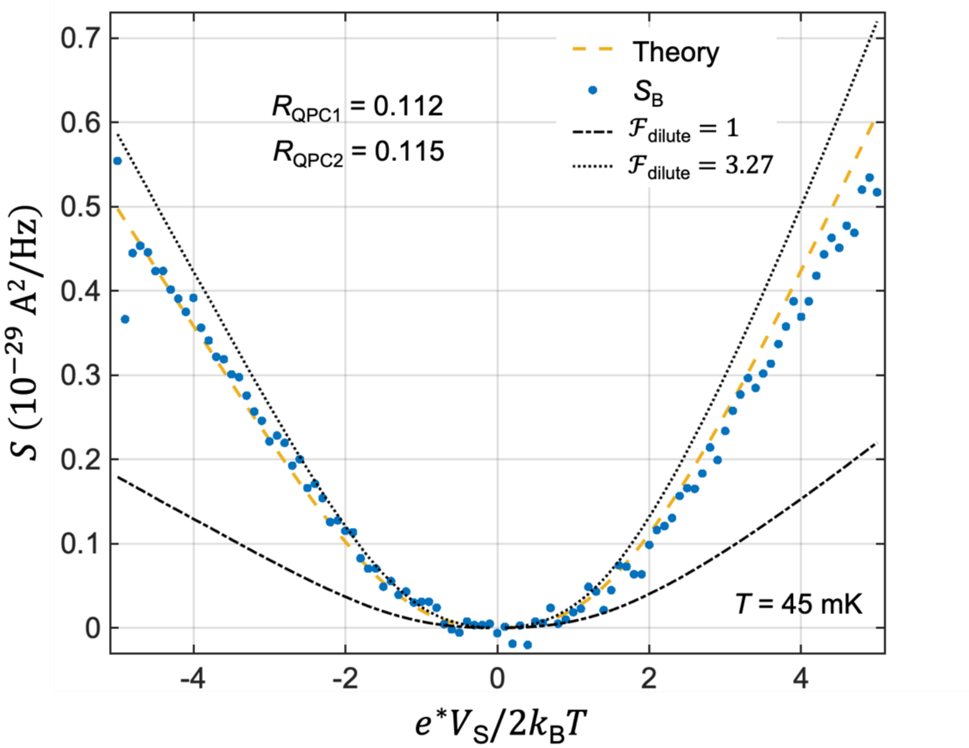

Figure 3. Excess auto-correlation noise measured at amplifier B (see Fig. 1a). A diluted beam of anyons is generated by reflection from QPC1 with probability R_{QPC1}=0.112. The dilute beam impinges on QPC2 with $R_{\mathrm{QPC2}} = 0.115$, creating excess auto-correlation (AC, shot noise) shown by the blue dots. The yellow dashed line corresponds to the prediction of the phenomenological model given by Eq.(2) in the main text, where $\mathcal{F}_{\mathrm{dilute}}$ is calculated based on the measured R_{QPC1} (Supplementary Sec. II & III). The dotted line corresponds to the time-domain braiding process which dominates over the trivial process, with Fano factor $\mathcal{F}_{\mathrm{dilute}} = 3.27$ (in the dilute limit $R_{\mathrm{QPC1}} \ll 1$). The black dashed/dotted line corresponds to $\mathcal{F}_{\mathrm{dilute}} = 1$, namely, the predicted noise when only trivial partitioning in QPC2 is considered.

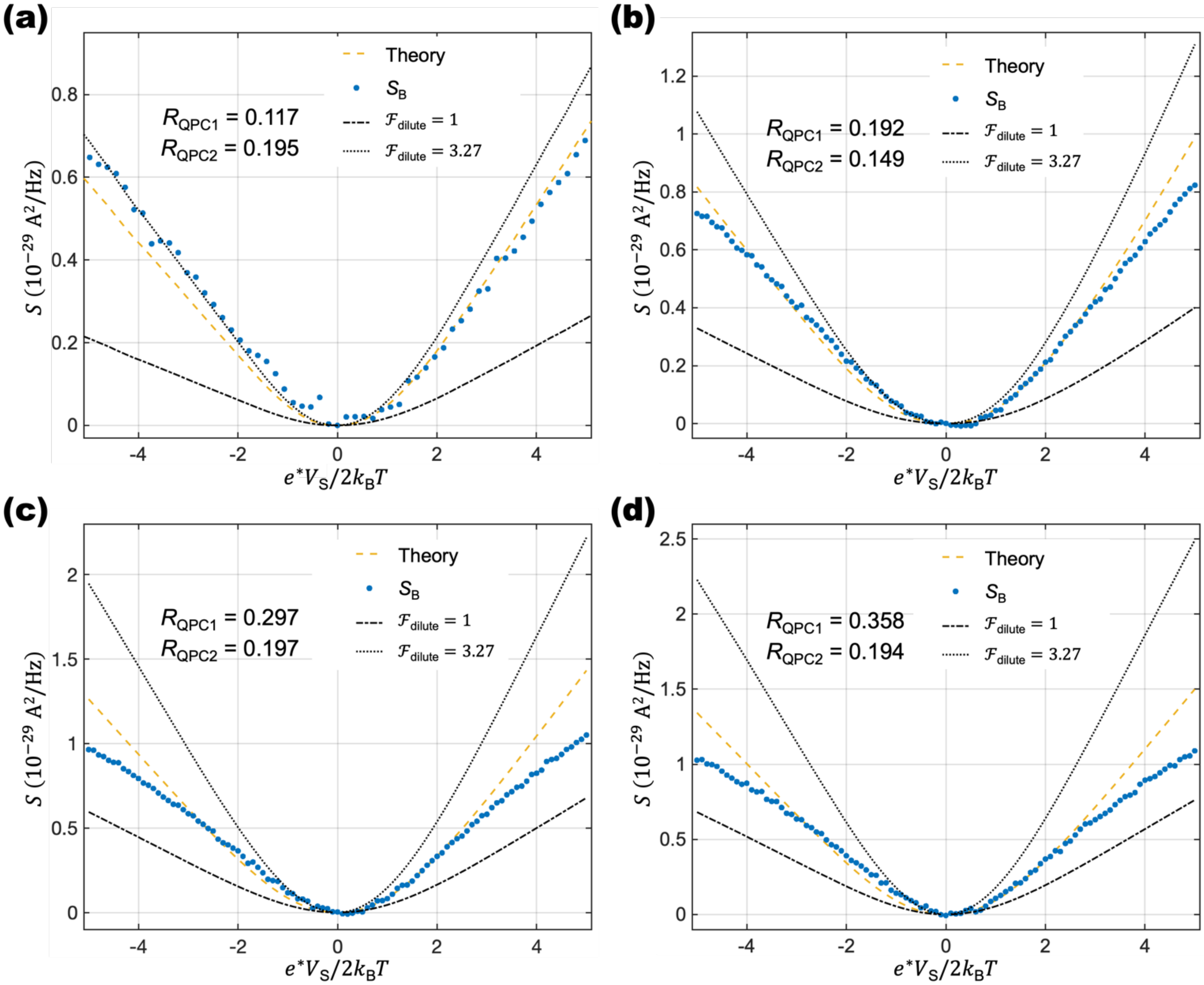

Figure 4. The dependence of the auto-correlation (amplifier B, Fig. 1a) on beam dilution (R_{QPC1}) and on R_{QPC2}. (a)-(d) are sorted from more to less dilution - the R_{QPC1} value. Excess auto-correlation (AC, shot noise) (blue dots) in the two-QPC geometry for different values of beam dilution. The yellow dashed lines are the theoretical predictions according to the phenomenological theory of Eq. (2) in the main text. The black dashed/dotted lines are according to the trivial process. The black dotted line is for the dilute limit where the primary contribution to the noise results from the time-domain braiding process. The data is in a good agreement with the theory over a wide range of parameters. As predicted by Eq. (3), a higher dilution (smaller R_{QPC1}) minimizes the impact of the trivial partitioning on the data, with the Fano factor of the AC approaching $\mathcal{F}_{\text{dilute}} = 3.27$.

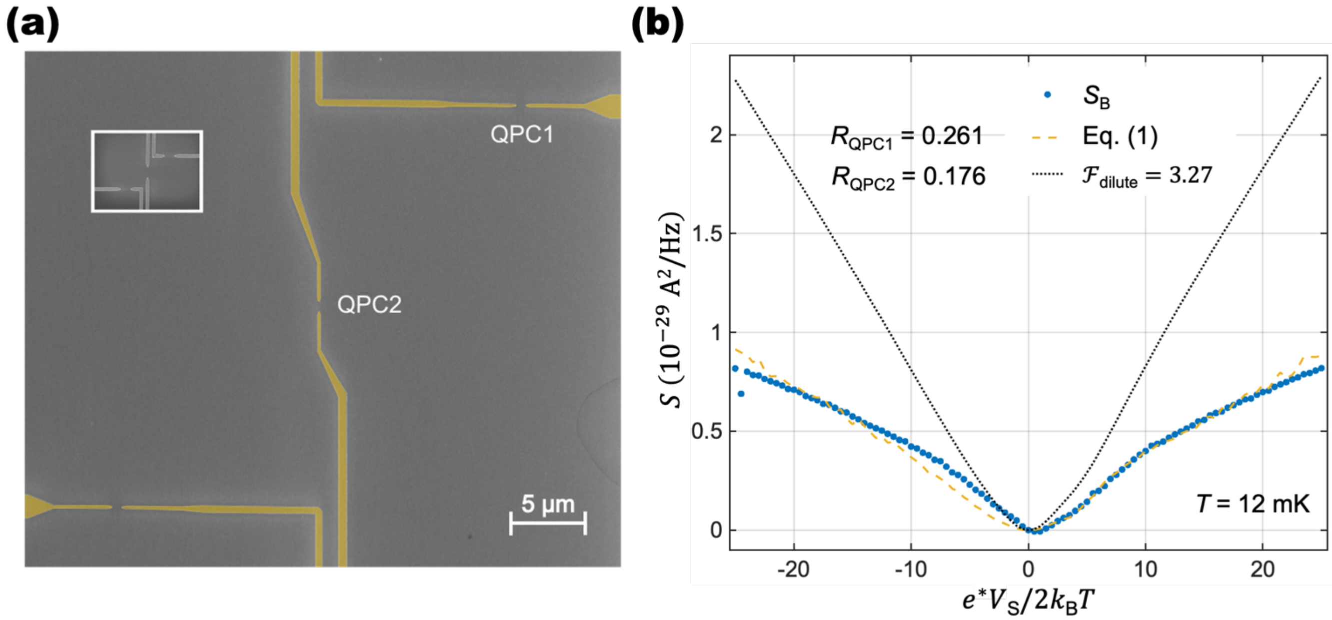

Figure 5. Two-QPC configuration with QPCs' distance of 20μm. (a) SEM image of the experimental setup. The gates are marked in yellow. The 2μm structure is shown (for comparison) in the white-bordered insert. **(b)** Blue dots: Measured excess auto-correlation with a dilution of $\boldsymbol{R_{\mathrm{QPC1}} = 0.261}$ and $\boldsymbol{R_{\mathrm{QPC2}} = 0.176}$, measured at 12mK. The measurement result agrees with the trivial model (i.e., integer filling factor), Eq. (1) with $\boldsymbol{R_{\mathrm{QPC1}} \rightarrow R_{\mathrm{QPC1}} R_{\mathrm{QPC2}}}$ – suggesting enrgy loss and dephasing. Black dotted line is the ideal anyonic behavior with Fano Factor $\boldsymbol{\mathcal{F}_{\mathrm{dilute}} = 3.27}$.

Supplementary Materials

Partitioning Diluted Anyons Reveals Their Braiding Statistics

June-Young M. Lee[1*], Changki Hong[2*], Tomer Alkalay[2*], Noam Schiller[2], Moty Heiblum[2], Yuval Oreg[2], H.-S. Sim[1]

[1]Department of Physics, Korea Advanced Institute of Science and Technology, Daejeon 34141, South Korea

[2]Department of Condensed Matter, Weizmann Institute of Science, Rehovot, Israel

*Equal Contribution

SI. EXPERIMENTAL SETUP DETAILS

The basis of our device is a high mobility GaAs-AlGaAs heterostructure that supports a two-dimensional electron gas (2DEG) 125 nm below the surface. The 2DEG has an electron density of 9.2×10^{10} cm^{-2}, and low temperature (4 kelvin) dark mobility of 3.9×10^{6} cm^{2}V^{-1}s^{-1}. Our experimental setup is shown in Fig. S1. Three Quantum Point Contacts (QPC) were patterned in close proximity and served as beam splitters in the measurement, ohmic contacts were used to source and collect the current. In the two-QPC setup, QPC1 dilutes the DC current I_S that is injected from source contact S1. The dilute reflected part of the current is then partitioned by QPC2. In the three-QPC setup, another source contact S2 is biased and injects DC current to the sample. Current from S2 is diluted by QPC3, and then fed into the second input of the QPC2. In both setups, the auto-correlation noise of each output beam, as well as the cross-correlation between the two outputs, are measured at a frequency of 730kHz set by the LC circuits. The signal was amplified by a home-made preamplifier cooled to $4.2K$ followed by a room temperature amplifier. The output of the amplification chain is then fed into a home-made analog cross-correlator circuit, which multiplies each signal with itself, as well as with the second signal. The output voltage from the analog cross-correlator was measured by digital multimeters. In order to calibrate the auto-correlation and cross-correlation measurements, we measured the shot noise of a full beam at an integer filling factor ($\nu = 3$). This was performed by fully pinching QPC1 while source contact is biased, such that only the QPC2 partitioned the beam. Comparing the auto-correlations and cross-correlations to Eq. (1) allowed us to calibrate our system. In addition, we repeated this measurement at $\nu = 1/3$, and made sure that both auto-correlations and the cross correlations leads to the correct fractional charge based on Eq. (1).

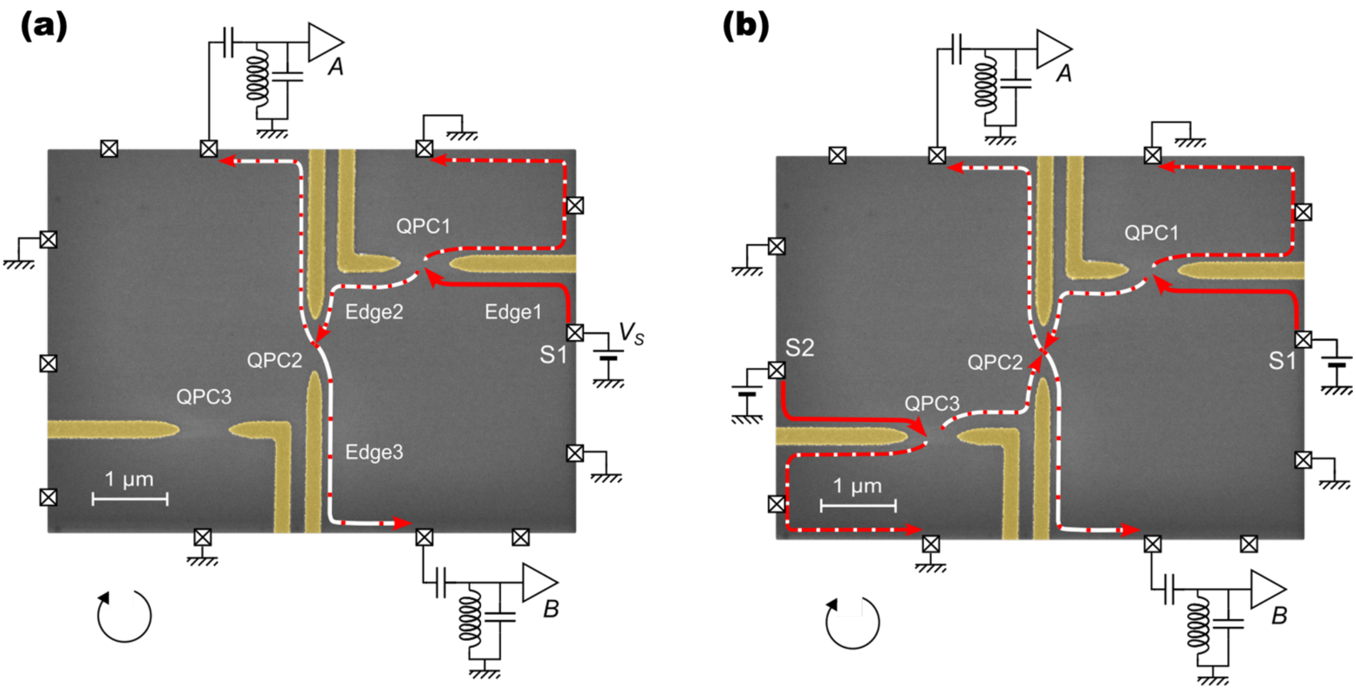

FIG. S1: **'Two-QPC' and 'three-QPC' geometries. (a)** A full beam is injected from source contact S1 and propagates along Edge1. The current is diluted by QPC1, the reflected part continues along Edge 2 and is partitioned by QPC2. **(b)** A second source (S2) is used to inject a full beam to QPC3, which is tuned such that it has the same tunneling probability as QPC1. The reflected current from QPC3 reaches the second input of QPC2. In both cases, the auto-correlation noise in each output beam is measured together with the cross-correlation between them.

SII. SUPPLEMENTARY DATA

A. Noise of a full beam impinging on QPC2

Here we compare the situation in which a dilute beam is injected to QPC2 (Fig. (3) in the main text) to that of a full beam injection. For the purpose, we utilized a second source contact [S2 contact in Fig. (S1)] to inject a full beam to QPC2, while QPC3 was fully pinched. QPC1 and QPC2 were held fixed at the same reflection used in the measurement of the dilute beam noise. As shown in Fig. S2, the noise follows Eq.(1) of the main text with charge $e^* \cong e/3$. This measurement emphasizes the remarkable difference between a full beam injection to a QPC and the dilute injection. In the former as Fig. S2, the Fano factor is sensitive only to the partitioned charge dominated by the trivial partitioning. In the latter as Fig. 3 in the main paper, the time-domain braiding takes over and the Fano factor becomes dependent on the braiding phase of anyons.

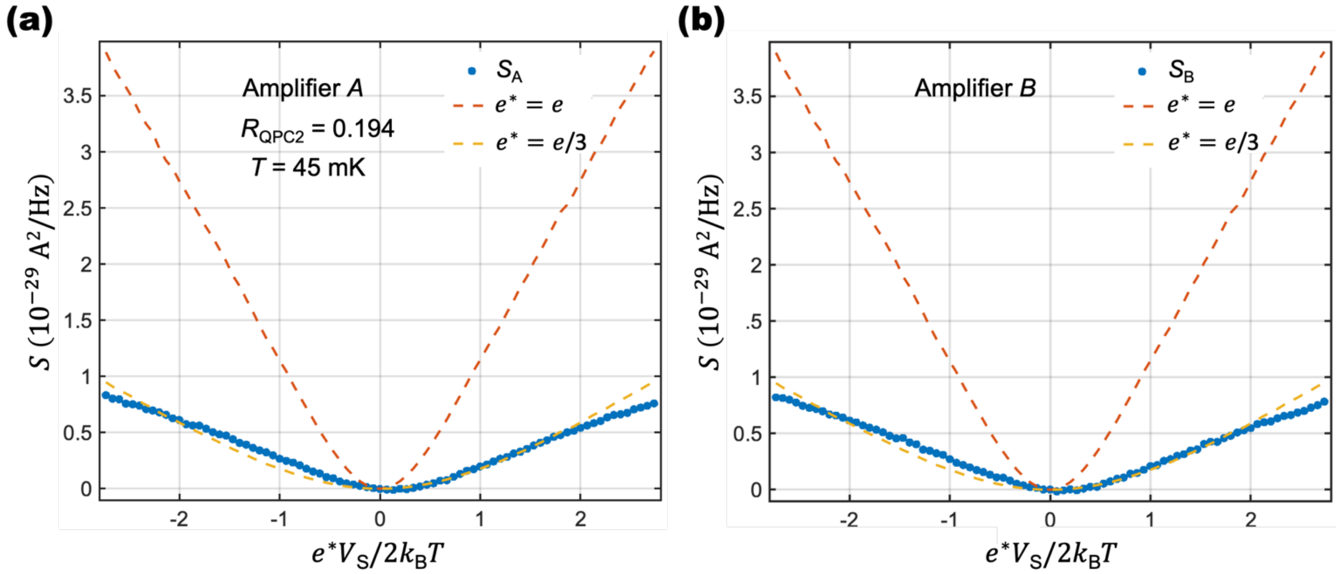

FIG. S2: **Noise of a full beam partitioned at QPC2.** A full beam is injected to QPC2 by biasing S2 and fully pinching QPC3. QPC1 and QPC2 were held at the same condition used to measure the noise of a dilute beam (R_{QPC2}=0.194). The AC noise at the two amplifiers (blue dots) is plotted together with the prediction of Eq. (1). The yellow dashed line is the expected noise with charge $e^* = e/3$, while the red dashed line shows the expected noise for $e^* = e$ for comparison. The data is in very good agreement with Eq. (1), demonstrating that the noise of a full beam is only sensitive to the charge of the partitioned particles. This should be contrasted with the noise of a dilute beam, shown in the main paper, where the Fano factor becomes a probe of the statistical phase due to contributions from the time-domain braiding process.

B. Two-QPC experiment in the IQH of filling factor 3

We performed the two-QPC experiment in the integer quantum Hall (IQH) regime, using the outer edge mode of filling factor 3. The condition is simpler (more ideal) to calculate because the DC bias dependency of the reflection probability is flat compared to other edges. In this regime, due to the trivial braiding phase of fermions, only the trivial partition process is expected to contribute to the noise, leading to $\mathcal{F}_{\text{dilute}} = 1$. In Fig. S3, we compare the measured auto-correlation noise at amplifier A and B with Eq.(1) (dashed lines in Fig. S3), with the electronic charge $e^* = e$ and R_{QPC1} replaced by the total probability to reach the amplifier such that for amplifier A, R_{QPC1} is replaced by $R_{\text{QPC1}}(1 - R_{\text{QPC2}})$, while for amplifier B, R_{QPC1} is replaced by $R_{\text{QPC1}}R_{\text{QPC2}}$. The theoretically expected values and the measurement results are in very good agreement, supporting that only the trivial partition process happens in the IQH.

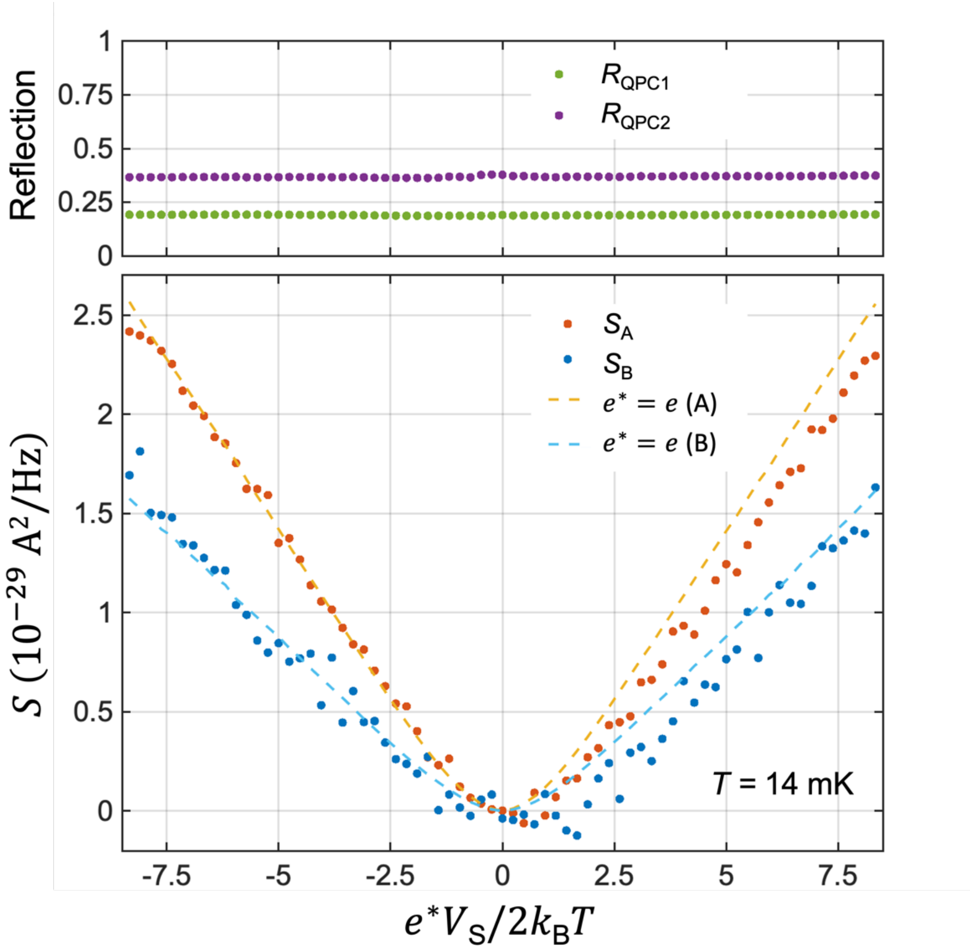

FIG. S3: **Excess auto-correlation noise in the two-QPC geometry at an integer filling factor ($\nu = 3$).** The upper panel shows the reflection probability of QPC1 and QPC2. In the lower panel, the red and blue dots are the measured AC noises at the two amplifiers. The red dashed line is the noise expected by Eq. (1), with the electronic charge $e^* = e$ and R_{QPC1} replaced by the combined probability to reach amplifier A, which is $R_{\text{QPC1}}(1 - R_{\text{QPC2}})$. Similarly, the blue dashed line is the expected noise at amplifier B with $e^* = e$ and $R_{\text{QPC1}} \rightarrow R_{\text{QPC1}}R_{QPC2}$. The agreement with the expected noise indicates that there is no additional contribution to the noise apart from the contribution of the trivial partitioning.

C. Bias dependence of the reflection

In the main text, each noise measurement is shown along with the average value of the reflection probability of each of the relevant QPC's. Here we show the full bias dependence of the reflection probabilities. Each panel of Fig. S4 shows the measured reflection probability for QPC1 (R_{QPC1}) and QPC2 (R_{QPC2}) and corresponds to one of the noise measurement presented in the main text. The corresponding noise measurement in the main text is written in the inset of each of the sub-figures. Figures S4 (a) to (e) measured at 45 mK, and Figure S4 (f) measured at 12 mK.

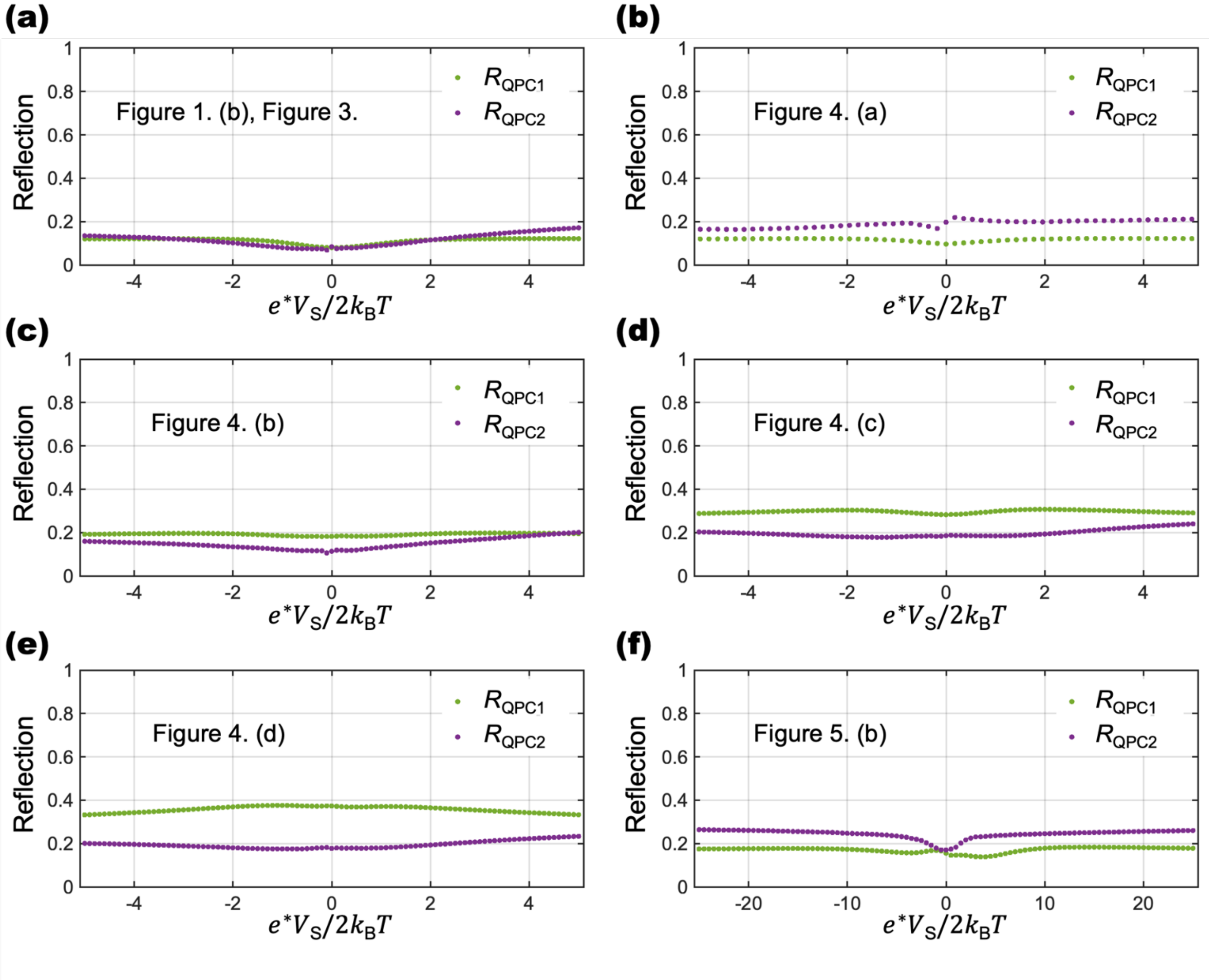

FIG. S4: **Bias dependence of the reflection probability.** Each of the panels **(a)**-**(f)** shows the full bias dependence of reflection probability measurement results for R_{QPC1} (green dots) and R_{QPC2} (purple dots). Each panel corresponds to noise measurement results in the main text: **(a)** corresponds to Fig. 1(b) and Fig. 3, **(b)** to Fig. 4(a), **(c)** to Fig. 4(b), **(d)** to Fig. 4(c), **(e)** to Fig. 4(d), and **(f)** to Fig. 5(b).

SIII. THEORY OF THE ANOMALOUS PARTITION NOISE

A. Fano factor $\mathcal{F}_{\text{dilute}}$

We provide the theory of the Fano factor $\mathcal{F}_{\text{dilute}}$ at sufficiently small R_{QPC2} and $e^*V_{\text{S}} \gg k_{\text{B}}T$. In Ref. [S1], the non-equilibrium correlator of anyon tunneling at QPC2 was derived for the dilute limit of $R_{\text{QPC1}} \ll 1$.

We first restate the result for Abelian anyons [S1]. The tunneling operator at QPC2 is expressed as $\mathcal{T}(t) = \gamma_2 \psi_3^\dagger(0,t)\psi_2(0,t)$, where $\psi_i(x,t)$ is the anyon annihilation operator on Edge$\boldsymbol{i}$ at position x and time t, and γ_2 is the tunneling strength at QPC2. For simplicity, the position of QPC2 is chosen as $x = 0$ on both Edge2 and Edge3. The non-equilibrium correlator of the tunneling operator $C_{\text{neq}}(t_1,t_2) \equiv \langle \mathcal{T}(t_1)\mathcal{T}^\dagger(t_2)\rangle_{\text{neq}}$ in the presence of the dilute anyon beam is related to the equilibrium correlator $C_{\text{eq}}(t_1,t_2) \equiv \langle \mathcal{T}(t_1)\mathcal{T}^\dagger(t_2)\rangle_{\text{eq}}$ in the absence of the beam,

$$C_{\text{neq}}(t_1,t_2) = e^{-\frac{I_{\text{QPC1}}}{e^*}\left(e^{i2\theta\,\text{sign}(t_2-t_1)}-1\right)|t_2-t_1|} C_{\text{eq}}(t_1,t_2) + \text{subleading terms.} \tag{S1}$$

This was derived with the firm theoretical ground based on the conformal field theory or the bosonization (the chiral Luttinger liquid (CLL) theory) for FQH edge channels, combined with the Keldysh perturbation theory for arbitrary orders of anyon tunneling at QPC1.

The multiplicative factor, the non-equilibrium part of the expression of $C_{\text{neq}}(t_1,t_2)$, is a consequence of time-domain anyon braiding. We found that the factor equals the average of the braiding phase $e^{2ik\theta}$ accumulated when the time-domain loop of a thermally excited anyon braids with k anyons of the dilute beam arriving at QPC2 in the time interval $t_2 - t_1$ ($\gg h/e^*\text{V}_{\text{S}}$),

$$\langle e^{2ik\theta}\rangle_{\text{Poissonian}} = \sum_{k=0}^{\infty} Q_k e^{2ik\theta} = e^{-\frac{I_{\text{QPC1}}}{e^*}\left(e^{2i\theta}-1\right)(t_2-t_1)}. \tag{S2}$$

The probability Q_k of the event of k anyons arriving at QPC2 in the interval $t_2 - t_1$ follows the Poissonian distribution $Q_k = \frac{m^k}{k!}e^{-m}$, and $m = I_{\text{QPC1}}(t_2 - t_1)/e^*$ is the average number of anyons arriving at QPC2 in the interval $t_2 - t_1$. The Poisson distribution is natural, since anyons of the dilute beam is generated by tunneling from Edge1 to Edge2 at QPC1 in the regime of $R_{\text{QPC1}} \ll 1$.

For a less dilute beam with relatively large R_{QPC1}, yet small enough for the anyon tunneling, it is natural to expect that the time distribution of anyons of the beam follows a binomial distribution, instead of the Poissonian distribution. Hence, in our phenomenological theory, we replace the multiplicative factor $\langle e^{2ik\theta}\rangle_{\text{Poissonian}}$ by the average braiding phase $\langle e^{2ik\theta}\rangle_{\text{binomial}}$ over the binomial distribution P_k of the number k,

$$\langle e^{2ik\theta}\rangle_{\text{binomial}} = \sum_{k=0}^{n} P_k e^{2ik\theta} = \left(1 - R_{\text{QPC1}} + R_{\text{QPC1}} e^{2i\theta}\right)^{I_{\text{S}}(t_2-t_1)/e^*} \tag{S3}$$

where $P_k = \frac{n!}{k!(n-k)!} R_{\text{QPC1}}^k \left(1 - R_{\text{QPC1}}\right)^{n-k}$, and $n = I_{\text{S}}(t_2 - t_1)/e^*$ is the number of anyons impinging at QPC1 on Edge1 in the time interval $t_2 - t_1$ ($\gg h/e^*\text{V}_{\text{S}}$). Using the factor, we write the non-equilibrium correlator

$$C_{\text{neq}}(t_1,t_2) = \left(1 - R_{\text{QPC1}} + R_{\text{QPC1}} e^{2i\theta\,\text{sign}(t_2-t_1)}\right)^{I_{\text{S}}|t_2-t_1|/e^*} C_{\text{eq}}(t_1,t_2) + \text{subleading terms.} \tag{S4}$$

This expression is also applicable to the case of $t_2 < t_1$, in which the braiding direction of the time-domain loop is opposite to the $t_2 > t_1$ case. Eq. (S4) reduces to the previous results of Eq. (S1) for $R_{\text{QPC1}} \ll 1$. This equation is valid for the long time regime $|t_2 - t_1| \gg h/e^*\text{V}_{\text{S}}$, where the spatial width of the wave packet of anyons in the dilute beam is sufficiently narrow so that the time-domain braiding is well-defined. The subleading terms describe the trivial partition process and become important in the short time regime of $|t_2 - t_1| \simeq h/e^*\text{V}_{\text{S}}$.

Once the non-equilibrium correlator is obtained, it is straightforward to calculate the tunneling rates $W_{2\to3}$ and $W_{3\to2}$,

$$W_{2\to3} = \int_{-\infty}^{\infty} dt \langle \mathcal{T}^\dagger(0)\mathcal{T}(t)\rangle_{\text{neq}}\,, \quad W_{3\to2} = \int_{-\infty}^{\infty} dt \langle \mathcal{T}(t)\mathcal{T}^\dagger(0)\rangle_{\text{neq}}\,. \tag{S5}$$

We first compute the contribution from the long time $|t_2 - t_1| \gg h/e^* V_S$ described by the time-domain braiding process,

$$\begin{aligned} W_{2\to3}^{\text{braid}} &= 2\frac{|\gamma_2|^2}{\hbar^2}\Gamma(1-2\delta)\text{Re}\left[e^{i\pi\delta}\left(-\frac{I_S}{e^*}\log\left(1+R_{\text{QPC1}}\left(e^{-2i\theta}-1\right)\right)\right)^{2\delta-1}\right], \\ W_{3\to2}^{\text{braid}} &= 2\frac{|\gamma_2|^2}{\hbar^2}\Gamma(1-2\delta)\text{Re}\left[e^{i\pi\delta}\left(-\frac{I_S}{e^*}\log\left(1+R_{\text{QPC1}}\left(e^{2i\theta}-1\right)\right)\right)^{2\delta-1}\right]. \end{aligned} \tag{S6}$$

Note that the only difference between the two rates is the braiding phase factor, $e^{-2i\theta} \leftrightarrow e^{2i\theta}$. This is explained by the fact that the the braiding direction of the time-domain loop is opposite between the processes of the two rates, particle tunneling from Edge2 to Edge3 for $W_{2\to3}^{\text{braid}}$ and hole tunneling from Edge2 to Edge3 for $W_{3\to2}^{\text{braid}}$. The time-domain braiding process contributes to the tunneling current and noise across QPC2 as $I_{\text{QPC2}}^{\text{braid}} = e^*\left(W_{2\to3}^{\text{braid}} - W_{3\to2}^{\text{braid}}\right)$ and $S_{\text{QPC2}}^{\text{braid}} = 2(e^*)^2\left(W_{2\to3}^{\text{braid}} + W_{3\to2}^{\text{braid}}\right)$,

$$\begin{aligned} I_{\text{QPC2}}^{\text{braid}} &= -4\frac{e^*}{\hbar^2}|\gamma_2|^2\Gamma(1-2\delta)\sin\pi\delta\,\text{Im}\left[\left(-\frac{I_S}{e^*}\log\left(1+R_{\text{QPC1}}\left(e^{-2i\theta}-1\right)\right)\right)^{2\delta-1}\right], \\ S_{\text{QPC2}}^{\text{braid}} &= 8\frac{e^{*2}}{\hbar^2}|\gamma_2|^2\Gamma(1-2\delta)\cos\pi\delta\,\text{Re}\left[\left(-\frac{I_S}{e^*}\log\left(1+R_{\text{QPC1}}\left(e^{-2i\theta}-1\right)\right)\right)^{2\delta-1}\right]. \end{aligned} \tag{S7}$$

If only the time-domain braiding determines the current and noise, the Fano factor $\mathcal{F}_{\text{dilute}}$ is written as

$$\mathcal{F}_{\text{dilute}} \simeq \frac{S_{\text{QPC2}}^{\text{braid}}}{2e^* I_{\text{QPC2}}^{\text{braid}}} = -\cot\pi\delta\,\frac{\text{Re}\left[\left(-\log\left(1+R_{\text{QPC1}}\left(e^{-2i\theta}-1\right)\right)\right)^{2\delta-1}\right]}{\text{Im}\left[\left(-\log\left(1+R_{\text{QPC1}}\left(e^{-2i\theta}-1\right)\right)\right)^{2\delta-1}\right]}. \tag{S8}$$

The dependence of $\mathcal{F}_{\text{dilute}}$ on the diluteness R_{QPC1} is plotted as the blue curve in Fig. S5. The Fano factor approaches to $\mathcal{F}_{\text{dilute}} \simeq 3.27$ in the Poissonian limit $R_{\text{QPC1}} \ll 1$, and decreases as the beam becomes less dilute.

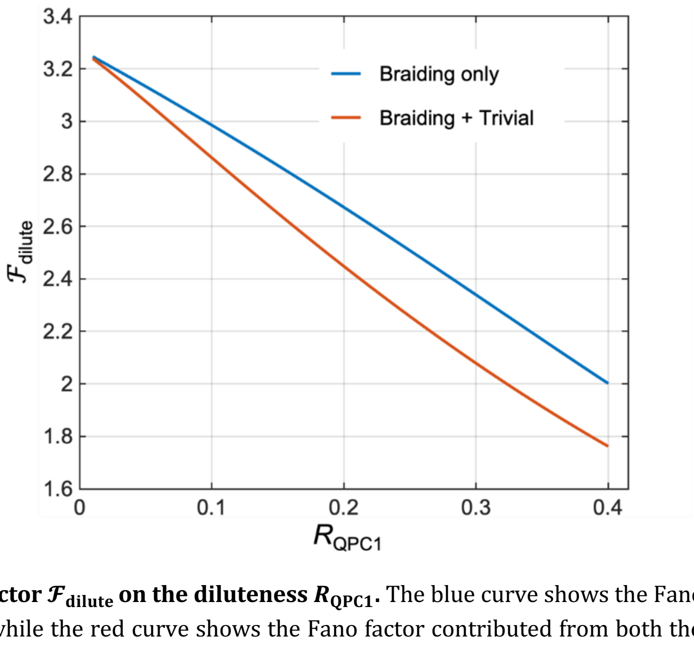

FIG. S5: **Dependence of Fano factor $\mathcal{F}_{\text{dilute}}$ on the diluteness R_{QPC1}.** The blue curve shows the Fano factor computed only with the time-domain braiding process, while the red curve shows the Fano factor contributed from both the time-domain braiding process and the trivial partition process.

There is also the trivial partition process, in which an anyon of the dilute beam directly tunnels at QPC2. This process occurs with the short time of $|t_2 - t_1| \simeq h/e^* V_\mathrm{S}$. It is sub-dominant in contributing to the current and noise at QPC2, and described by the subleading terms in Eq. (S1) and Eq. (S4),

$$\text{the sub-leading terms of Eq. (S1) and Eq. (S4)} \simeq \frac{e}{e^*}\frac{\Gamma(2\delta)}{\Gamma(\delta)^2} R_\mathrm{QPC1} e^{-ie^* V_\mathrm{S}(t_1-t_2)/\hbar} C_\mathrm{eq}(t_1, t_2)\,. \tag{S9}$$

Using this, the contribution of the trivial partition process to the current and noise at QPC2 is obtained,

$$I_\mathrm{QPC2}^\mathrm{trivial} = e^* W_{2\to 3}^\mathrm{trivial} = R_\mathrm{QPC1} \times \frac{2\pi e|\gamma_2|^2}{\hbar^2 \Gamma(\delta)^2}\left(\frac{2\pi I_\mathrm{S}}{e}\right)^{2\delta-1}, \quad S_\mathrm{QPC2}^\mathrm{trivial} = 2e^* I_\mathrm{QPC2}^\mathrm{trivial}\,. \tag{S10}$$

For the dilute limit $R_\mathrm{QPC1} \ll 1$, the contribution of the trivial process is sub-dominant compared to that of the braiding process,

$$\frac{\text{contribution of the trivial partition}}{\text{contribution of the time-domain braiding}} \propto R_\mathrm{QPC1}^{2-2\delta}. \tag{S11}$$

We note that if there were only the trivial partition process, the Fano factor has the value of $\mathcal{F}_\mathrm{dilute} = S_\mathrm{QPC2}^\mathrm{trivial}/(2e^* I_\mathrm{QPC2}^\mathrm{trivial}) = 1$ [see Eq. (S10)], as discussed in the main text.

The total current and noise at QPC2 are $I_\mathrm{QPC2} = I_\mathrm{QPC2}^\mathrm{braid} + I_\mathrm{QPC2}^\mathrm{trivial}$ and $S_\mathrm{QPC2} = S_\mathrm{QPC2}^\mathrm{braid} + S_\mathrm{QPC2}^\mathrm{trivial}$, where both the time-domain braiding process and the trivial partition process are taken into account. The full Fano factor is

$$\mathcal{F}_\mathrm{dilute} = \frac{S_\mathrm{QPC2}}{2e^* I_\mathrm{QPC2}} = \frac{S_\mathrm{QPC2}^\mathrm{braid} + S_\mathrm{QPC2}^\mathrm{trivial}}{2e^*\left(I_\mathrm{QPC2}^\mathrm{braid} + I_\mathrm{QPC2}^\mathrm{trivial}\right)}. \tag{S12}$$

The dependence of the full Fano factor on R_QPC1 is shown as the red curve in Fig. S5. As the contribution of the trivial partition process becomes larger (yet smaller than that of the braiding process) for larger R_QPC1, the Fano factor further decreases.

B. Phenomenological extension in Eq. (2)

In the last subsection, we have derived $S_\mathrm{QPC2} = \mathcal{F}_\mathrm{dilute} \times 2e^* I_\mathrm{QPC2}$ for high voltage $e^* V_\mathrm{S} \gg k_\mathrm{B} T$ and small QPC2 reflection $R_\mathrm{QPC2} \ll 1$. We now phenomenologically extend it to the form in Eq. (2) of the main text, to compare the result with our experimental data in a wider range of the parameters. We restate the equation,

$$S_\mathrm{QPC2} = \mathcal{F}_\mathrm{dilute} \times 2e^* I_\mathrm{QPC1} R_\mathrm{QPC2}(1 - R_\mathrm{QPC2})\left[\coth\left(\frac{e^* V_\mathrm{S}}{2k_\mathrm{B}T}\right) - \frac{2k_\mathrm{B}T}{e^* V_\mathrm{S}}\right]. \tag{S13}$$

We here provide the rationale behind the extension.

Firstly, $[\coth(e^* V_\mathrm{S}/2k_\mathrm{B}T) - 2k_\mathrm{B}T/e^* V_\mathrm{S}]$ is introduced to describe a parameter range of relatively small values of voltage V_S. The factor $\coth(e^* V_\mathrm{S}/2k_\mathrm{B}T)$ comes from the hole-like anyon injection process at the QPC1 [S2]. It can be considered that the hole-like anyons are incoming from the source to QPC1 with a rate $I_\mathrm{S}\exp(-e^* V_\mathrm{S}/k_\mathrm{B}T)/e^*$, which is exponentially suppressed in comparison with the particle-like anyon injection. The hole-like anyon injection affects both the time-domain braiding process and the trivial partition process. In the time-domain braiding process, when a hole-like anyon is injected at QPC1 to the dilute beam flowing along Edge2, the time-domain loop of a thermally excited anyon at QPC2 can braid the hole-like anyon, giving rise to the braiding phase factors of $e^{\pm 2i\theta}$, instead of the factors $e^{\mp 2i\theta}$ of the case of the particle-like anyon injection in Eq. (S4). As a result, the first term of the non-equilibrium correlator in Eq. (S4) has an additional multiplicative factor of $\left(1 - R_\mathrm{QPC1} + R_\mathrm{QPC1} e^{-2i\theta \mathrm{sign}\,(t_2 - t_1)}\right)^{\frac{I_\mathrm{S}}{e^*}\exp\left(-\frac{e^* V_\mathrm{S}}{k_\mathrm{B}T}\right)|t_2 - t_1|}$ coming from the hole-like anyon injection. Then the current and noise at QPC2 are modified accordingly. On the other hand, in the trivial partition process, the hole-like anyon injection modifies the current and noise at QPC2 as $I_{\mathrm{QPC2}}^{\mathrm{trivial}} \rightarrow I_{\mathrm{QPC2}}^{\mathrm{trivial}}\left(1-\exp\left(-\frac{e^*V_{\mathrm{S}}}{k_{\mathrm{B}}T}\right)\right)$ and $S_{\mathrm{QPC2}}^{\mathrm{trivial}} \rightarrow S_{\mathrm{QPC2}}^{\mathrm{trivial}}\left(1+\exp\left(-\frac{e^*V_{\mathrm{S}}}{k_{\mathrm{B}}T}\right)\right)$. The Fano factor $\mathcal{F}_{\mathrm{dilute}}$ is then calculated by $\mathcal{F}_{\mathrm{dilute}} = \frac{S_{\mathrm{QPC2}}}{2e^*I_{\mathrm{QPC2}}\coth(e^*V_{\mathrm{S}}/2k_{\mathrm{B}}T)}$. The last term of Eq. (S13) proportional to $-2k_{\mathrm{B}}T/e^*V_{\mathrm{S}}$ is introduced to make the excess noise to vanish at the zero bias of $V_{\mathrm{S}}=0$. Note that all the temperature dependence is introduced from the detailed balance principle, while we used the zero-temperature correlator of the CLL theory in the calculation of $\mathcal{F}_{\mathrm{dilute}}$. This phenomenological treatment is in analogy to the full beam case [S2], which remedies the power-law temperature dependence of the CLL theory that disagrees with experiments.

Secondly, we did the substitution of R_{QPC2} to $R_{\mathrm{QPC2}}(1-R_{\mathrm{QPC2}})$ to obtain Eq. (S13). With this substitution, a parameter range of relatively large values of R_{QPC2} is described by Eq. (S13). This is done in the same spirit with the phenomenological expression of Eq.(1) for the partition of a full beam, where the substitution of R_{QPC1} to $R_{\mathrm{QPC1}}(1-R_{\mathrm{QPC1}})$ has been performed [S3] to have comparison between experimental data and the phenomenological expression in determination of fractional charges by shot noise, going beyond the parameter regime of the chiral Luttinger liquid theory. Excellent agreement between the phenomenological expression in Eq. (S13) (namely Eq. (2) of the main text) with our experimental data is found as shown in Fig. 3 & 4 of the main text.

C. Dependence of Fano factor $\mathcal{F}_{\mathrm{dilute}}$ on the scaling dimension δ

While the chiral Luttinger liquid theory predicts the power law behavior $R_{\mathrm{QPC}} \propto V^{2\delta-2}$ of the reflection probability R_{QPC} at a QPC with respect to a bias voltage V, this expected behavior has not been confirmed by experiments [S4]. As the Fano factor $\mathcal{F}_{\mathrm{dilute}}$ of our theory also depends on the scaling dimension δ, it is in fact surprising that the excellent agreement between the theory and our experiment is found over a wide range of the parameters. To understand why, we investigate how $\mathcal{F}_{\mathrm{dilute}}$ varies as a function of the scaling dimension δ. For simplicity, we concentrate on the high voltage regime of $e^*V_{\mathrm{S}} \gg k_{\mathrm{B}}T$.

For the Poissonian limit of $R_{\mathrm{QPC1}} \ll 1$, the time-domain braiding process dominates the trivial partition process, and the Fano factor is written concisely,

$$\mathcal{F}_{\mathrm{dilute}} = -\cot\pi\delta\cot\left(\left(\frac{\pi}{2}-\theta\right)(2\delta-1)\right). \tag{S14}$$

As non-ideal effects at QPCs usually affect the scaling dimension δ to become larger than its ideal value 1/3 at ν = 1/3 [S5, S6], we explore how the Fano factor varies as δ increases from the ideal value. The result is shown as the blue curve in Fig. S2. As δ increases, the Fano factor decreases from the ideal value ($\simeq$ 3.27) at δ = 1/3 to 3 at δ = 1/2, and increases back to the original value at δ = 2/3. It shows that the Fano factor varies less than 10 % over the range of 1/3 < δ < 2/3. This may in part explain the excellent agreement between the theory and the experiment.

Next we take the realistic value of $R_{\mathrm{QPC1}}=0.1$, as in Fig. 3 of the main text. If we consider the time-domain braiding process only, $\mathcal{F}_{\mathrm{dilute}}$ starts from 3.13 at δ = 1/3, reduces to 2.87 at δ = 1/2, and increases back to the original value 3.13 at δ = 2/3 (see the red curve in Fig. S6). Again, the variation of $\mathcal{F}_{\mathrm{dilute}}$ is less than 10% over the range of δ. The variation becomes bigger if we also include the trivial partition process. It starts from 3.08 at δ = 1/3 and decreases monotonically to 2.36 at δ = 2/3 (see the yellow curve in Fig. S6). In this case, the difference becomes about 20%. The relatively big variation is because the trivial process is less suppressed for larger δ, as expected from the ratio $R_{\mathrm{QPC1}}^{2-2\delta}$ of the contribution of the trivial process to that of the braiding process shown in Eq. (S11). Still, however, the variation is not that strong compared to the variation range of δ.

Nevertheless, our transmission data are nearly flat, corresponding to δ = 1 (Supplementary Section SII C). With δ = 1, the Fano factor in Eq. (S14) diverges and cannot explain our experimental results. This suggests to revisit the long-time issue of whether and how the scaling dimension can be obtained from experimental data of the voltage dependence of QPC transmission. For example, the QPC model Hamiltonian used in the chiral Luttinger liquid theory for the prediction of the voltage dependence (the power-law behavior $R_{\mathrm{QPC}} \propto V^{2\delta-2}$ of the QPC reflection probability R_{QPC} on a voltage V)

might be too simplified; while the bare anyon-tunneling strength at a QPC has been assumed to be energy independent in the theory, it could be energy dependent in realistic situations, which distorts the predicted power-law behavior even when the scaling dimension remains around the ideal value. Or, measurements of other quantities might be useful for experimental identification of the scaling dimension (see, e.g., Ref. [S8]).

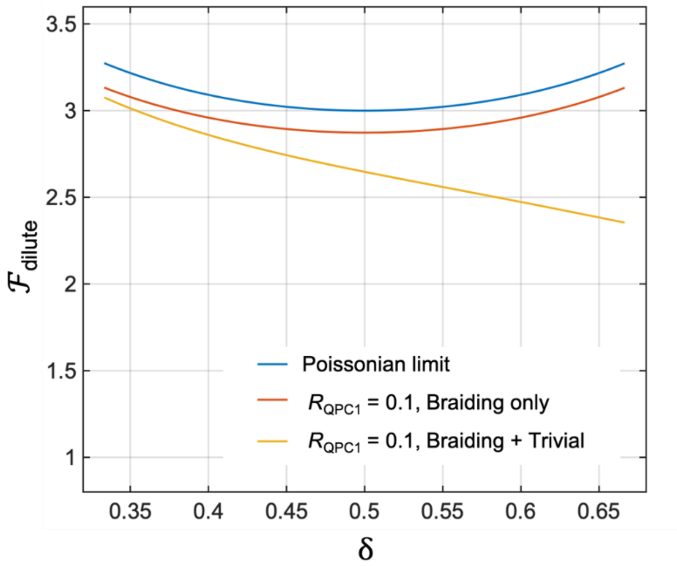

FIG. S6: **Dependence of Fano factor $\mathcal{F}_{\text{dilute}}$ on the scaling dimension δ.** The blue curve is for the Poissonian limit, while the red and yellow curves are for $R_{\text{QPC1}} = 0.1$. In the red curve, only the time-domain braiding process is taken into account, while the yellow curve accounts both the braiding process and the trivial partition process.

SIV. COMPARISON BETWEEN S_{B} AND S_{QPC2}

Below we show that the measured excess AC noise S_{B} at amplifier B provides the direct probe of the theoretical prediction of the excess AC S_{QPC2} at QPC2.

The excess AC S_{B} at amplifier B and the excess AC S_{QPC2} at QPC2 are related [S9] as

$$S_{\text{B}} = S_{\text{QPC2}} + 4k_{\text{B}}TG\left[\left.\frac{\partial I_{\text{QPC2}}}{\partial V_3}\right|_{V_3=0} - \left.\frac{\partial I_{\text{QPC2}}}{\partial V_3}\right|_{V_3=V_{\text{S}}=0}\right], \tag{S15}$$

where $G = \nu e^2/h$. The second term of Eq. (S15) is obtained by lock-in measurement with a small variation of a voltage V_3 applied to S2 while pinching QPC3 completely off, in the presence of the voltage V_{S} on Edge1. The third term is the same quantity with the second, but it is obtained in the absence of V_{S}. These terms correspond to the correlation between the tunneling current across QPC2 and the current flowing along Edge3.

The difference between S_{B} and S_{QPC2} is small at high voltage $e^*V_{\text{S}} \gg k_{\text{B}}T$. Moreover, as excess noises are the quantities of interest, the difference is even more negligible; the third term partly cancels the second term in Eq. (S15). This is explicitly shown in Fig. S7. This shows that the measured excess noise S_{B} provides the direct probe of the theoretical prediction of S_{QPC2}.

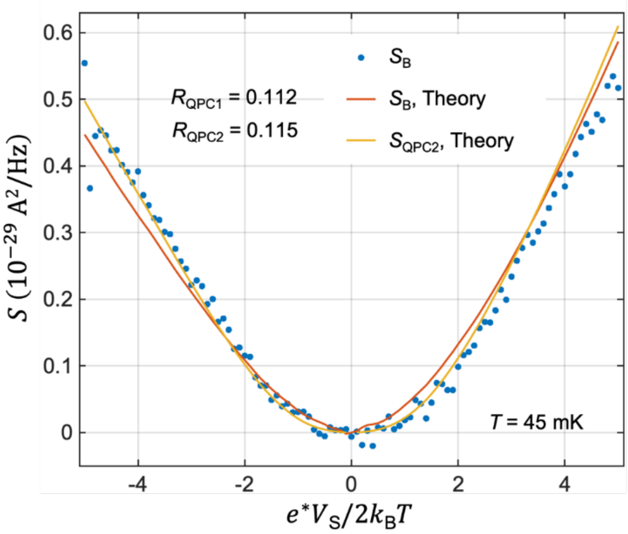

FIG. S7: $\boldsymbol{S_{\mathrm{B}}}$ **and** $\boldsymbol{S_{\mathrm{QPC2}}}$. The difference between S_{B} and S_{QPC2} is sufficiently small. The same data set with Fig. 3 of the main text is used.

SV. TWO-QPC EXPERIMENT AT FILLING FACTOR $\nu = 2/5$

In this supplementary section, we extend our study to the FQH regime at ν = 2/5. Its edge structure is composed of two (inner and outer) edge channels. The inter-QPC distance is 2 μm.

First, we performed a two-QPC experiment on the outer edge channel, making the inner edge channels fully reflected at the QPCs. In the same way with Fig. 1(b), we confirmed that the tunneling charge at QPC1 is $e^* = e/3$ [Fig. S8(a)], as expected. We observed that partitioning of diluted anyons of the fractional charge at QPC2 results in the Fano factor close to $\mathcal{F}_{\mathrm{dilute}}$ = 3.27 as in ν = 1/3 [Fig. S8(b)]. The Fano factor agrees well with our theory based on the braiding angle $2\theta = 2\pi/3$ and the scaling dimension $\delta = 1/3$, supporting the time-domain braiding process also in the outer edge channel at ν = 2/5.

Next, we performed another two-QPC experiment on the inner edge channel, making the outer edge channels fully transmitted through the QPCs. The tunneling charge at QPC2 was found as $e^* = e/5$ from the shot noise measurement where a full beam impinges at QPC2 while QPC1 is pinched off [Fig. S9(a)]. Then, partitioning a dilute beam at QPC2, we obtained $\mathcal{F}_{\mathrm{dilute}} \sim 1$ in our measurement uncertainty (which suffers from the very weak spectral density, weaker than the ν = 1/3 case). The result implies that the trivial partition process is more substantial along the inner channel.

We compare the experimental result of partitioning the inner channel with existing theoretical models. There are several models for edges at ν = 2/5. In the model by Wen [S11] where large spatial separation between the inner and outer channels is considered, anyons with fractional charge $e^* = e/5$ have the braiding phase $2\theta = 6\pi/5$ and scaling dimension δ = 3/5. This model supports $\mathcal{F}_{\mathrm{dilute}} \simeq -5.16$ when only the time-domain braiding process is considered and $\mathcal{F}_{\mathrm{dilute}} \simeq 30$ when both the time-domain braiding and the trivial partition processes are considered with the measured value of $R_{\mathrm{QPC1}} = 0.088$. Hence it is incompatible with our experiment. Another model proposed by Lopez and Fradkin [S12] predicts a downstream charge mode and non-propagating neutral modes. In this case, the braiding phase is solely from the propagating downstream charge mode, and it has the value of $2\theta = \pi/5$. And, the two δs appearing in Eq. (S14) become to have different values; the first one is $8/5$ and the second is $1/10$. This is because the non-propagating neutral mode contributes to the anyonic exchange phase at a QPC, but not to its tunneling exponent. The resulting Fano factor is $\mathcal{F}_{\text{dilute}} \simeq -0.2$, which cannot explain our experiment. On the other hand, Ferraro *et al.* [S13] modified the Lopez-Fradkin model. In their model, there is a downstream charge mode and upstream neutral modes. Then, while the most relevant tunneling charge at a QPC at low temperature is $e^* = 2e/5$ (which is described by $2\theta = 4\pi/5$ and $\delta = 2/5$), there is another quasiparticle tunneling of charge $e^* = e/5$ (described by $2\theta = \pi/5$ and $\delta = 8/5$). Since our experimental data support $e^* = e/5$ and it is expected that the quasiparticle of $e^* = e/5$ has larger bare QPC tunneling strength than that of $e^* = 2e/5$, we assumed that the anyon with $e^* = e/5$ dominates the QPC tunneling in our experiment. Our theory shows that this anyon results in the Fano factor $\mathcal{F}_{\text{dilute}} \simeq 1$, since the large scaling dimension $\delta = 8/5$ (> 1) makes the trivial partition process to dominate over the braiding process [See Eq. (S11)]. This may explain our experiment on partitioning the inner edge channel. There might be also a possibility that interactions between the channels give rise to decoherence effects in favor of the trivial partition process.

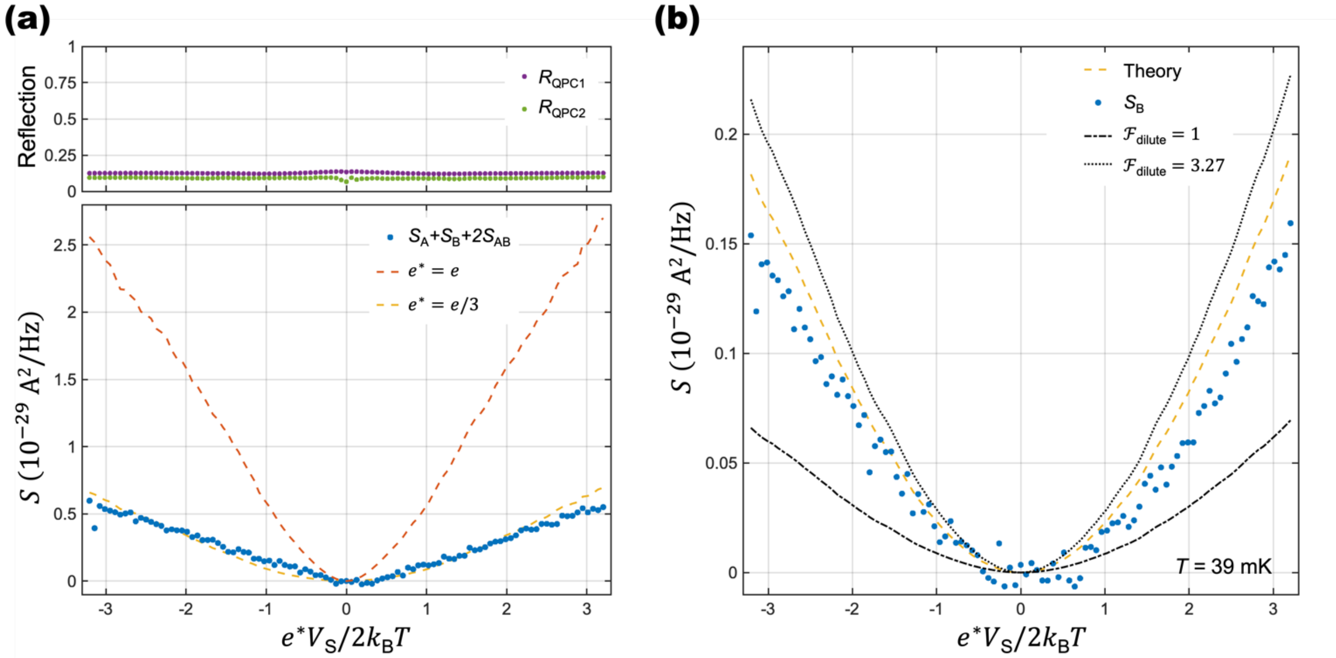

FIG. S8: **Noise measurement for ν = 2/5 outer edge. (a)** Upper panel: Reflection probabilities R_{QPC1} (purple dots) and R_{QPC2} (green dots). Lower panel: Measurement of tunneling charge at QPC1. Blue dots are $S_A + S_B + 2S_{AB}$ noise calculation from measurement. Red dashed line and yellow dashed line are obtained from Eq. (1) in the main text, with $e^* = e$ and $e^* = e/3$ respectively. **(b)** Dilute beam impinges on QPC2, creating the excess AC. The reflection probabilities of the QPCs are the same as (a).

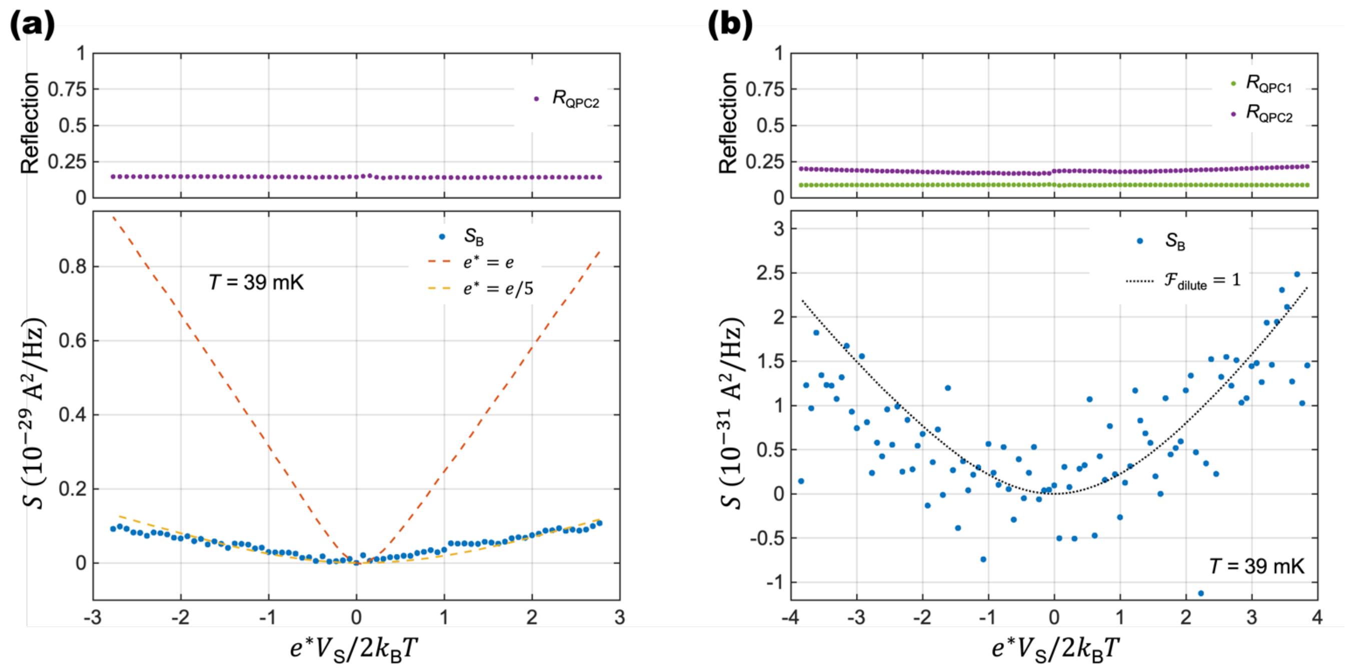

FIG. S9: **Noise measurement for ν = 2/5 inner edge. (a)** QPC1 is pinched off for injecting a full beam to QPC2. Upper panel: Reflection probability R_{QPC2} for the inner edge. Lower panel: Auto-correlation shot noise measurement results (blue dots) at 39 mK. Red dashed line and yellow dashed line are obtained from Eq. (1) in the main text, with $e^* = e$ and $e^* = e/5$ respectively. **(b)** Two-QPC experiment result. Upper panel: Reflection probability R_{QPC1} (green dots) and R_{QPC2} (purple dots). Lower panel: The measured excess noise S_{B} (blue dots). The black dotted line corresponds to Eq. (2) with $\mathcal{F}_{\text{dilute}} = 1$.

SVI. CROSS CORRELATION

Here, we show that our experimental data of the cross correlation (CC) S_{AB} of the two-QPC setup and an additional three-QPC setup are also in excellent agreement with our theory mainly based on the time-domain braiding process. For the two-QPC setup, the CC S_{AB} between amplifiers A and B is related to the AC noise of QPC2 by

$$S_{\text{AB}} = -S_{\text{QPC2}} + \frac{\partial I_{\text{QPC2}}}{\partial I_{\text{QPC1}}} S_{\text{QPC1}}\,, \tag{S16}$$

where the second term corresponds to the correlation between the tunneling current I_{QPC1} at QPC1 and the tunneling current I_{QPC2} at QPC2 [S1, S7]. For comparison between our experimental data and the theory, we replace the differential reflection $\partial I_{\text{QPC2}}/\partial I_{\text{QPC1}}$ by its averaged value R_{QPC2}. Then S_{AB} is obtained by using S_{QPC2} in Eq. (S13) and S_{QPC1} in Eq.(1) of the main text. This theoretical result is in good agreement with our experimental data [Fig. S10(a)]. For comparison, we also cite the free fermion results from the Landauer-Büttiker formalism, which corresponds to the trivial partition,

$$S_{\text{AB}} = -2e^* I_S R_{\text{QPC1}}^2 R_{\text{QPC2}}\left(1 - R_{\text{QPC2}}\right)\left[\coth\left(\frac{e^* V_{\text{S}}}{2k_B T}\right) - \frac{2k_B T}{e^* V_S}\right], \tag{S17}$$

and plot it in Fig. S10(a) as the red dashed line with $e^* = e/3$.

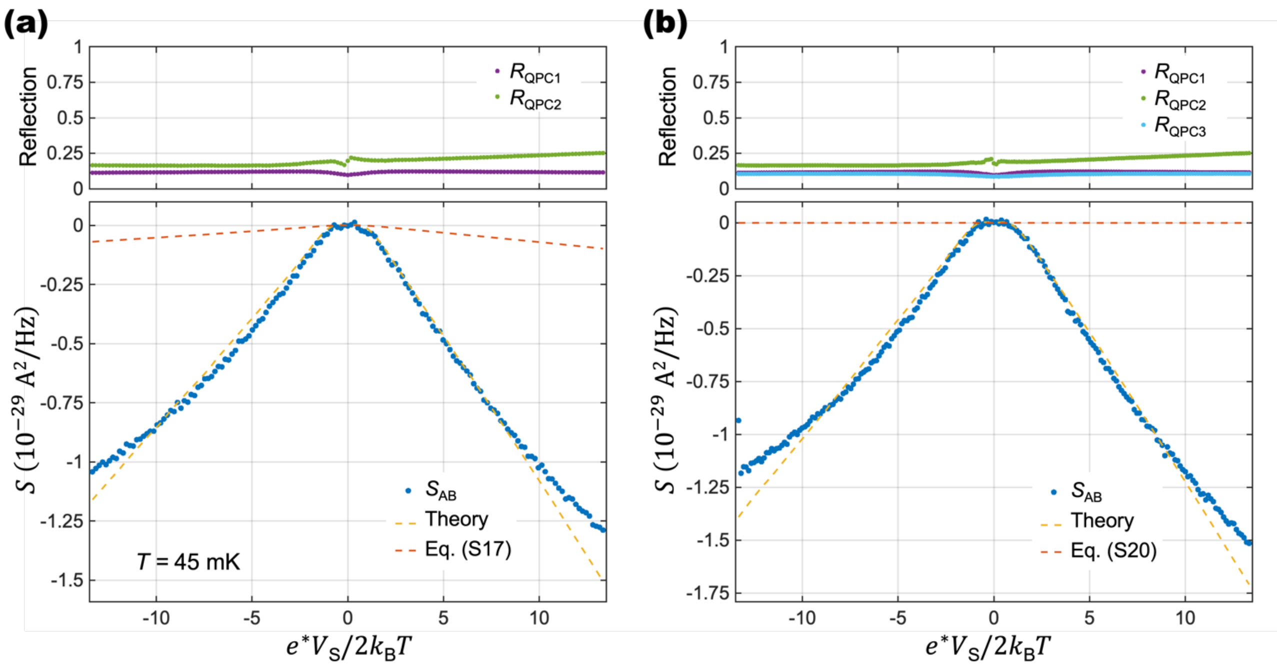

FIG. S10: **Cross correlations (a)** Cross correlation S_{AB} of the two-QPC geometry. **(b)** S_{AB} of the three-QPC geometry with symmetric injection of two dilute beams to QPC2. The experimental data of **(a)** were obtained with the same measurement (e.g., R_{QPC1}, R_{QPC2}) with Fig. 4(a) of the main text. The data of **(b)** were obtained with the average value of $R_{QPC1} = 0.116$, $R_{QPC2} = 0.192$, and $R_{QPC3} = 0.102$. The results are in good agreement with our theoretical result (yellow dashed lines). The results of Eq. (S17) and Eq. (S20) for the trivial partition process (red dashed lines) are shown for comparison.

We also analyze our experimental data of the CC S_{AB} of a three-QPC geometry [Fig. S1(b)], which is essentially the same configuration with Ref. [S10]. To have the three-QPC geometry, we operated an additional QPC, QPC3, located downside of QPC2. This QPC connects Edge3 with an additional edge channel, Edge4, via anyon tunneling. By applying a voltage of the same amplitude V_S to the source contact S2 with that applied to the source contact S1 of Edge1, a current I_S flows along Edge4 (the same amount with the current along Edge1). It is reflected at QPC3, then a dilute beam of current $I_{QPC3} = R_{QPC3} I_S$ is generated to flow along Edge3 towards QPC2, where R_{QPC3} is the reflection probability at QPC3. So the two dilute beams, one along Edge2 and the other along Edge3, are injected to QPC2. Then the CC S_{AB} between amplifiers A and B was measured.

Theoretically, the CC is written as

$$S_{AB} = -S_{QPC2} + \frac{\partial I_{QPC2}}{\partial I_{QPC1}} S_{QPC1} - \frac{\partial I_{QPC2}}{\partial I_{QPC3}} S_{QPC3}\,, \tag{S18}$$

where $S_{QPC3} = 2e^* I_S R_{QPC3}(1 - R_{QPC3}) \left[\coth\left(\frac{e^*V_S}{2k_BT}\right) - \frac{2k_BT}{e^*V_S}\right]$ is the excess tunneling noise at QPC3 following Eq. (1). The third term is the correlation between the tunneling currents I_{QPC2} and I_{QPC3}. As in our phenomenological theory for the two-QPC setup, we calculated the noise S_{QPC2} as

$$S_{QPC2} = \mathcal{F}_{\mathrm{dilute}} \times 2e^* \left|I_{QPC1} - I_{QPC3}\right| R_{QPC2}(1 - R_{QPC2}) \left[\coth\left(\frac{e^*V_S}{2k_BT}\right) - \frac{2k_BT}{e^*V_S}\right]. \tag{S19}$$

The Fano factor $\mathcal{F}_{\mathrm{dilute}} = S_{QPC2}/2e^* I_{QPC2}$ is calculated by the CLL theory for $R_{QPC2} \ll 1$ and $e^*V_S \gg k_BT$ as before. The non-equilibrium correlator in Eq. (S4) has the multiplicative factor in the first term, which describes the effect of the dilute beam injected across QPC1. In the case of the two dilute beams, the non-equilibrium correlator is modified such that the first term has an additional multiplicative factor of $\left(1 - R_{QPC3} + R_{QPC3} e^{-2i\theta \mathrm{sign}\,(t_2 - t_1)}\right)^{\frac{I_S}{e^*}|t_2 - t_1|}$ which describes the effect of the dilute beam injected across QPC3. We note that the braiding phase factor $e^{-2i\theta \mathrm{sign}\,(t_2 - t_1)}$ of this multiplicative factor for the dilute beam injected across QPC3 differs from the factor $e^{2i\theta \mathrm{sign}\,(t_2-t_1)}$ of the multiplicative factor for the dilute beam injected across QPC1, because the time-domain loop at QPC2 braids the two beams in the opposite direction to each other. Using the modified non-equilibrium correlator, it is straightforward to compute the tunneling current and noise at QPC2, hence, the Fano factor $\mathcal{F}_{\mathrm{dilute}}$.

Note that in the case of the perfectly symmetric injection of $I_{\mathrm{QPC1}} = I_{\mathrm{QPC3}}$, $\mathcal{F}_{\mathrm{dilute}}$ diverges, and Eq. (S19) is invalid. However, Eq. (S18) is applicable to our experimental situation where there was about 10% difference between R_{QPC1} and R_{QPC3} [Fig. S10(b)] so that both $I_{\mathrm{QPC1}} - I_{\mathrm{QPC3}}$ and $\mathcal{F}_{\mathrm{dilute}}$ are finite.

For comparison between our experimental data and the theory, we replace the differential reflections $\partial I_{\mathrm{QPC2}}/\partial I_{\mathrm{QPC1}}$ and $-\partial I_{\mathrm{QPC2}}/\partial I_{\mathrm{QPC3}}$ in Eq. (S17) by their averaged value R_{QPC2}. Then S_{AB} is obtained by using S_{QPC2} in Eq. (S19), S_{QPC1} in Eq. (1) of the main text and an equation for S_{QPC3} corresponding to Eq. (1). This theoretical result is in good agreement with our experimental data [Fig. S10(b)]. The excellent agreement between our phenomenological theory and our measurement of the CC S_{AB} strongly supports that the time-domain braiding process is the underlying mechanism in both the two- and three-QPC geometries. Note that we also plot the non-interacting results from the Landauer-Büttiker formalism with the trivial partition process (with $e^* = e/3$),

$$S_{\mathrm{AB}} = -2e^* I_S (R_{\mathrm{QPC1}} - R_{\mathrm{QPC3}})^2 R_{\mathrm{QPC2}} (1 - R_{\mathrm{QPC2}}) \left[\coth\left(\frac{e^* V_{\mathrm{S}}}{2k_B T}\right) - \frac{2k_B T}{e^* V_S}\right], \tag{S20}$$

as the red dashed line in Fig. S10(b) for comparison.

Last but not least, we point out that measurement of AC S_{B} at the port B in the two-QPC geometry is more useful for detecting the time-domain anyon braiding at QPC2 than the CC S_{AB}, especially for the case of non-Abelian anyons. It is firstly because S_{B} is more directly related to the noise S_{QPC2} at QPC2 where the time-domain braiding process happens. As shown in Eq. (S15), S_{B} becomes the same with S_{QPC2} as the temperature becomes lower. By contrast, the difference between the CC S_{AB} and S_{QPC2} is not negligible, as the second term of Eq. (S16) is of the same order with S_{QPC2}. Secondly, in the most promising non-Abelian FQH states, upstream and downstream flows coexist along FQH edges. Then, there can occur some side-effects by the coexistence [S1]. The ratio of the side-effects compared to the main signal of our interest is of the order of $R_{\mathrm{QPC1}} R_{\mathrm{QPC2}}$ for the case of S_{B}, but it is of the order of R_{QPC1} for the case of S_{AB}. The AC S_{B} is more robust against the side-effects than CC S_{AB}.

[S1] J.-Y. M. Lee and H.-S. Sim, Non-Abelian Anyon Collider, arXiv:2202.03649 (2022).

[S2] D. E. Feldman and M. Heiblum, Why a noninteracting model works for shot noise in fractional charge experiments, Phys. Rev. B **95**, 115308 (2017).

[S3] For a review, see M. Heiblum, in Perspectives of Mesoscopic Physics: Dedicated to Yoseph Imry's 70th Birthday, edited by A. Ahrony and O. Entin-Wohlman (World Scientific, Singapore, 2010).

[S4] D. C. Glattli, Tunneling Experiments in the Fractional Quantum Hall Regimes. In: Douçot, B., Pasquier, V., Duplantier, B., Rivasseau, V. (eds) The Quantum Hall Effect. Progress in Mathematical Physics, vol 45. Birkhäuser Basel (2005).

[S5] B. Rosenow and B. I. Halperin, Nonuniversal Behavior of Scattering between Fractional Quantum Hall Edges, Phys. Rev. Lett. **88**, 096404 (2002).

[S6] A. Braggio, D. Ferraro, M. Carrega, N. Magnoli, and M. Sassetti, Environmental induced renormalization effects in quantum Hall edge states, New J. Phys. **14**, 093032 (2012).

[S7] B. Rosenow, I. P. Levkivskyi, and B. I. Halperin, Current Correlations from a Mesoscopic Anyon Collider. Phys. Rev. Lett. **116**, 156802 (2016).

[S8] N. Schiller, Y. Oreg, and K. Snizhko, Extracting the scaling dimension of quantum Hall quasiparticles from current correlations, Phys. Rev. B **105**, 165150 (2022).

[S9] B. Lee, C. Han, and H.-S. Sim, Negative Excess Shot Noise by Anyon Braiding. Phys. Rev. Lett. **123**, 016803 (2019).

[S10] H. Bartolomei *et al.*, Fractional statistics in anyon collisions, Science **368**, 6487 (2020).

[S11] X.-G. Wen, Topological orders and edge excitations in fractional quantum Hall states, Adv. Phys. 44, 405 (1995).

[S12] A. Lopez and E. Fradkin, Universal structure of the edge states of the fractional quantum Hall states, Phys. Rev. B **59**, 15323 (1999).

[S13] D. Ferraro, A. Braggio, M. Merlo, N. Magnoli, and M. Sassetti, Relevance of Multiple Quasiparticle Tunneling between Edge States at ν = p/(2np + 1), Phys. Rev. Lett. **101**, 166805 (2008).